APETALA2 functions as a temporal factor together with BLADE-ON-PETIOLE2 and MADS29 to control flower and grain development in barley

Shoesmith, Jennifer; Solomon, Charles Ugochukwu; Yang, Xiujuan; Wilkinson, Laura G.; Sheldrick, Scott; van Eijden, Ewan

Published in:
Development

DOI:
10.1242/dev.194894

Publication date:
2021

Document Version
Peer reviewed version

APETALA2 functions as a temporal factor together with *BLADE-ON-PETIOLE2* and *MADS29* to control flower and grain development in barley

Jennifer R. Shoesmith[1,2], Charles Ugochukwu Solomon[3,4*], Xiujuan Yang[5*], Laura G. Wilkinson[5,6], Scott Sheldrick[1], Ewan van Eijden[1], Sanne Couwenberg[1], Laura Pugh[1], Mhmoud Eskan[1], Jennifer Stephens[2], Abdellah Barakate[2], Sinéad Drea[3], Kelly Houston[2], Matthew R. Tucker[5**] and Sarah M. McKim[1]**

*authors contributed equally

**corresponding authors

[1]Division of Plant Sciences, School of Life Sciences, University of Dundee at the James Hutton Institute, Invergowrie, DD2 5DA, UK

[2]Cell and Molecular Sciences, The James Hutton Institute, Invergowrie, DD2 5DA, UK

[3]Department of Genetics and Genome Biology, University of Leicester, University Road, Leicester LE1 7RH, UK

[4]Department of Plant Science and Biotechnology, Abia State University, PMB 2000, Uturu, Nigeria.

[5]Waite Research Institute, University of Adelaide, Waite Campus, Urrbrae, SA, Australia

[6]John Innes Centre, Norwich Research Park, Norwich, NR4 7UH, UK

Key words

Barley, AP2, Floret, Grain, CRISPR/Cas9, MADS-box, BOP1/2, B-sister, nucellus, integument

ABSTRACT

Cereal grain develops from fertilised florets. Alterations in floret and grain development greatly influence grain yield and quality. Despite this, little is known about the underlying genetic control of these processes, especially in key temperate cereals such as barley and wheat. Using a combination of near-isogenic mutant comparisons, gene editing and genetic analyses, we reveal that *HvAPETALA2* (*HvAP2*) controls floret organ identity, floret boundaries, and maternal tissue differentiation and elimination during grain development. These new roles of HvAP2 correlate with changes in grain size and HvAP2-dependent expression of specific *HvMADS-box* genes, including the B-sister gene, *HvMADS29*. Consistent with this, gene editing demonstrates that *HvMADS29* shares roles with *HvAP2* in maternal tissue differentiation. We also discovered that a gain-of-function *HvAP2* allele masks changes in floret organ identity and grain size due to loss of barley *LAXATUM.A*/*BLADE-ON-PETIOLE2* (*HvBOP2*) gene function. Taken together, we reveal novel, pleiotropic roles and regulatory interactions for an *APETALA2*-like gene controlling floret and grain development in a temperate cereal.

INTRODUCTION

Sex in angiosperms occurs in the flower, a complex structure of multiple organs whose coordinated growth leads to production of seed. Double fertilisation of the embryo sac within the ovary generates two filial seed tissues, the embryo and endosperm, which proliferate and expand while enclosed by layers of maternal ovary tissue, including the proximal, nutritive nucellus and the more distal integuments that form the protective seed coat (Wilkinson *et al.*, 2018). The grass flower or 'floret' ovary is additionally encircled by the ovary wall or pericarp which with the underlying maternal and filial tissues grow into the grain fruit or 'caryopsis'. The caryopsis isotopically expands following fertilisation and then elongates and swells to fill the cavity between opposing floret hulls (Brinton & Uauy, 2019). Several genes that regulate ovary, nucellus, integument, pericarp and/or hull development also influence grain size (Song *et al.*, 2007; Yin & Xue, 2012; Brinton *et al.*, 2017; Ren *et al.*, 2018; Zhao *et al.*, 2018; Wilkinson *et al.*, 2019). However, the mechanism used by these genes to influence grain size is poorly understood. This problem has major translational significance in cultivated cereal grasses whose endosperm provides more calories than any other source to the human diet.

Learning more about the genetic and functional networks in the floret and grain may help to dissect this problem. Each floret arises from a floret meristem made by the spikelet, the basic reproductive unit of grasses. Floret meristems form opposing lemma and palea hulls which enclose the stamens and single-ovary carpel (Schrager-Lavelle et al., 2017). Small sacs called lodicules develop between the lemma and stamens which enlarge at anthesis (pollen shed), prising open the lemma to facilitate pollen transfer (Kellogg, 2015). Molecular patterns controlling floret morphogenesis appear partially conserved with the ABCDE gene combinatorial model proposed to explain flower development in dicots such as *Arabidopsis thaliana* (Schrager-Lavelle *et al.*, 2017). In the Arabidopsis flower, activity of class 'A' genes defines the outer perianth (sepals), 'AB', the inner perianth (petals), 'BC', the

stamens, 'C', the carpel, and 'CD' the ovule, with the 'E' class genes contributing to all other class functions (Theißen *et al.*, 2016; Irish, 2017). Other than the 'A' class *APETALA2* (*AP2*) gene, the ABCDE genes encode MADS-box transcription factors. Orthologous *MADS-box* expression in rice suggests that the palea and lemma are analogous to sepals (Lombardo & Yoshida, 2015) while the lodicules are highly-derived petals (Yoshida, 2012). Lemma formation also represents a commitment of the axillary meristem to floret fate (Arber, 2010; Kellogg, 2015). Thus, grass perianth development involves decisions about organ identity and spikelet versus floret fate.

Specific genes establishing floret and organ identity in grasses are not completely resolved, especially in temperate cereals such as barley and wheat that develop unbranched 'spike' inflorescences. However, the A-class *APETALA2-like* (*AP2L*) genes and their regulation by microRNA172 (miR172) appears to play a central role. In spikes, spikelets directly attach to the spike axis at alternating nodes flanked by two bract-like glumes. In wheat, miR172-resistant alleles of *TaAP2L5* (the *Q* domestication gene) or *TaAP2L2* cause glume to lemma transformations, ectopic florets and compact spikes, while overexpression of miR172, or loss of *TaAP2L5* or *TaAP2L2* function, leads to longer spike internodes, glume-like lemmas and reiterations of empty glumes (Simons *et al.*, 2006; Sormacheva *et al.*, 2015; Debernardi *et al.*, 2017, 2020; Greenwood *et al.*, 2017). These phenotypes suggest that *TaAP2L*s promote lemma identity and floret establishment, a role partially conserved in rice based on loss of function phenotypes of the *SUPERNUMERARY BRACT* (*SNB*) and *INDETERMINATE SPIKELET1* (*IDS1*) *AP2L*-genes (Lee *et al.*, 2007; Lee & An, 2012; Ji *et al.*, 2019). In barley, a gain-of-function *HvAP2* allele called *Zeo1.b* disrupts miR172-directed *HvAP2* transcript cleavage, elevating *HvAP2* transcript levels and leading to small, non-swelling lodicules, semi-dwarfism and dense spikes (Houston *et al.*, 2013; Patil *et al.*, 2019). We do not know whether *HvAP2* fulfils similar roles as *TaAP2L5* or *TaAP2L2* in floret establishment or organ identity. The only gene currently identified that controls floret organ identity in barley is the *LAXATUM.A*/ *HvBLADE-ON-PETIOLE2* (*HvBOP2*) gene encoding a transcription factor necessary for lodicule identity and

repression of spike internode elongation (Jost et al., 2016). The regulatory mechanism(s) of HvBOP2 and its relationship to *HvAP2* or the ABCDE model are unknown.

AP2L genes also regulate post-fertilisation development across different plants. In Arabidopsis, *AtAP2* restricts integument cell expansion, seed size and seed mass (Modrusan *et al.*, 1994; Jofuku *et al.*, 1994; Ohto *et al.*, 2005) while in rice, *SNB* limits grain size and weight, a role associated with constraining floret hull cell expansion (Jiang *et al.*, 2019; Ma *et al.*, 2019). Whether *AP2L* genes also control post-fertilisation development in temperate cereals is unexplored. Here, we identify and characterise a new *HvAP2* allele in the barley Bowman Near-Isogenic Line (BWNIL) mutant population (Druka et al., 2011) and generate additional alleles by gene editing to reveal both conserved and novel roles for *HvAP2* in floret and grain development.

RESULTS

BW381 (*gigas1.a*) shows altered floret organ identity and growth

To learn more about HvAP2, we screened the BWNILs for loss of function *HvAP2* alleles, focusing on mutants with introgressions that overlapped *HvAP2* (Druka *et al.*, 2011; Houston *et al.*, 2013). We selected the BW381 line containing the *gigas1.a* locus (Greek for giant), originally isolated in the cultivar (*cv.*) Golden Melon (Tsuchiya, 1962; Franckowiak, 1995; Druka *et al.*, 2011; Table S1). BW381 (hereafter called *gigas1.a*) showed multiple elongated features compared to the recurrent parent *cv.* Bowman (Fig. 1; Table S2). Spike internodes were longer ($p=0.036$), causing less dense or *laxatum* spikes, glumes were 20% longer ($p=0.028$), and lemmas and paleas were 50% longer ($p\leq0.001$) shifting the *gigas1.a* spikelet shape from wedge to lance-shaped (Fig. 1A-D,F,G; Fig S1A-C; Table S2). Adaxial lemma epidermal cell length in *gigas1.a* was 52% increased compared to Bowman ($p\leq0.001$, Fig. S1D), suggesting that increased cell elongation explained longer *gigas1.a* lemmas, although these cells were also 16% wider compared to Bowman ($p\leq0.001$, Fig S1E). In Bowman and most

cultivated barleys, lemmas and glumes tips have thin projections called awns; the lemma awn is longer with a distinct boundary from the lemma (Fig. 1C,E). Glume awns in *gigas1.a* were 50% longer compared to those of Bowman ($p<0.001$; Fig. 1C,E,G; Table S2) yet lemma awns in *gigas1.a* were 23% shorter ($p\leq0.001$), with a less distinct lemma-awn boundary (Fig. 1C,E,F; Table S2), two glume awn-like features. Lodicules in *gigas1.a* developed ectopic distal lamina (Fig. 1H, I), associated with extreme open-flowering (Fig. S1F), decorated with glume-like hairs (Fig. 1J; Fig. S1G,H). We observed that *gigas1.a* stigmas had fewer, shorter papillae branches in contrast to feathery 'plumose' stigmas of Bowman (Fig. 1K), which may contribute to reduced seed set in *gigas1.a*, as previously reported (Tsuchiya, 1962). Grain length in *gigas1.a* mirrored the longer hulls and increased by 47% compared to Bowman ($p\leq0.001$; Fig. 1L–N; Table S2). Pericarp epidermal cells in *gigas1.a* were only 16% longer compared to Bowman, as well as 23% wider ($p\leq0.001$; Fig. S2B,C), suggesting that changes in grain length likely involves increases in cell size and cell number. However, *gigas1.a* thousand grain weight (TGW) increased only 7% since *gigas1.a* grain was also narrower and thinner compared to Bowman ($p\leq0.001$; Fig. 1M; Fig. S2; Table S2), although its lemma width was unchanged (Fig. S1A). Caryopses in *gigas1.a* were darker than Bowman (Fig. 1M), suggesting increased proanthocyanidins in the seed coat (Aastrup *et al.*, 1984). We re-examined *Zeo1.b* for additional phenotypes, finding that *Zeo1.b* glumes often transform into lemmas (Fig. 1O) and that *Zeo1.b* grain is 8% wider compared to Bowman ($p\leq0.001$; Fig. S2; Table S2). While we did not observe differences in cell length or width in the adaxial lemma of *Zeo1.b*, the pericarp cells were 52% wider compared to Bowman ($p\leq0.001$Fig S2C), suggesting that HvAP2 promotes medial cell expansion in the barley pericarp. Taken together, elongated glume-like organs, expanded cells, lax spikes, open-flowering, and longer grain of *gigas1.a* contrasted with the closed-flowering, compressed growth, glume to lemma transformation and wider grain of *Zeo1.b*.

gigas1.a phenotypes result from a deletion of _HvAP2_

Given the opposing phenotypes to *Zeo1.b*, we speculated that *gigas1.a* may be a loss of function *HvAP2* allele. To clone the locus, we first placed the BOPA2 markers associated with the *gigas1.a* introgression on the physical map (Mascher *et al.*, 2017) which located a Golden Melon introgression on 2H between 710843099bp and 758851055bp (Fig. S3). Testing *gigas1.a* genomic DNA on the barley 50K iSelect SNP Array (Bayer *et al.*, 2017) identified a slightly larger area on 2H from 710163110bp to 760762651bp (Fig. 2A; Table S3). SNPs starting after 729506693bp and ending between 730687131bp and 730852717bp on 2H were present in Golden Melon and Bowman appeared as missing in *gigas1.a*, demarked an area encompassing *HvAP2* (HORVU2Hr1G113880.23) and six other high confidence genes (Fig. 2A; Table S3, S4). Using *gigas1.a* genomic DNA, we successfully amplified two genes outside this region but could not amplify *HvAP2* or two other genes in this region (Fig. S3). We detected *HvAP2* transcripts in Bowman and *Zeo1.b* spikes but not *gigas1.a* (Fig. 2B). Collectively, our evidence suggests that a deletion on 2H in *gigas1.a* removed *HvAP2* and at least six other genes.

To our knowledge, *gigas1.a* was the only available *gigas1* allele. To confirm that *gigas1.a* phenotypes do not result from the deletion of genes other than *HvAP2*, we targeted the *HvAP2* gene using CRISPR/Cas9 gene editing. We transformed Golden Promise with two binary vectors containing the *bcoCas9* (barley codon optimised Cas9) sequence and one guide RNA sequence targeting *HvAP2* sequences upstream of those encoding the first AP2 DNA-binding domain (Fig. 2C). Screening 18 independent T_1 transformants identified two new *HvAP2* alleles, *hvap2-1* and *hvap2-2*, with a 39bp and 40bp deletions, respectively, in the first exon (Fig. 2C). The *hvap2-1* deletion (175bp to 214bp relative to the coding sequence start) removed 13 amino acids (residues 60-73) before the first AP2 domain in the predicted protein but kept the remaining sequence in frame (Fig. 2C). We observed no obvious morphological differences in *hvap2-1* compared to Golden Promise (Fig. 2D–F). The *hvap2-2* deletion (175bp–215bp) removed the same 13 amino acids but also caused a frame shift and a premature stop codon in exon 5 (368bp), predicted to significantly impair HvAP2 function (Fig. 2C). The *hvap2-2* mutant largely phenocopied *gigas1.a*, with longer lemmas ($p \leq 0.001$), lax spikes

(p=0.005) and long, slender grain compared to Golden Promise (Fig. 2D,E; Fig. S4; Table S3). We note that in this experiment, *gigas1.a* had marginally wider lemmas compared to Bowman (Fig S4A, $p<0.05$). Lodicules in *hvap2-2* were larger, extended and swollen compared to the non-swelling lodicules of Golden Promise (Fig. 2F), a cleistogamous cultivar with the *Zeo2* allele (Houston et al., 2013). Green organs with a hybrid composition of stamen-like filaments and smooth and hairy bract-like regions replaced the lodicules in 3% of *hvap2-2* florets (Fig. 2G,H), a more severe loss of lodicule identity compared to *gigas1.a*, potentially reflecting the different cultivar backgrounds. Overall *hvap2-2* closely phenocopied *gigas1.a*, corroborating that *gigas1.a* phenotypes result from deletion of *HvAP2* alone. Thus, we propose that HvAP2 defines the boundary between the glume and lemma (outer perianth), promotes floret perianth identity, increases stigmatic papillae branching and widens grain, while also restricting longitudinal growth of spike internodes, spikelets, floret organs and grain.

HvAP2 functions during early floral development

We compared early spikelet development in Bowman, *Zeo1.b* and *gigas1.a* to understand when and how HvAP2 influences organ identity. We staged floret organ development using the Waddington (WD) stages (Waddington et al., 1983). WD4 stage *Zeo1.b* spikelets exhibited wider glumes than Bowman, leading to two interlocking lemma-like organs (Fig. 3A) which later overgrew the floret lemma (Fig. 3B). Lodicule primordia emerged similarly in Bowman, *gigas1.a* and *Zeo1.b* at WD4 but by WD5.5, WD7 and later, Bowman lodicules displayed distinct proximal cushion and distal fringe tissues (Fig. 3C, Fig. S5). In contrast, *gigas1.a* lodicules were flatter with distal extensions while *Zeo1.b* lodicules remained small, lacked cushions, and formed hairs (Fig. 3C; Fig. S5). These data suggest that *HvAP2* and its miR172-regulation between WD4 and WD7 influence early spikelet differentiation.

194 AtAP2 controls Arabidopsis floral organ development in part through regulating *MADS-box* gene
195 expression (Drews *et al.*, 1991; Yant *et al.*, 2010; Dinh *et al.*, 2012). We hypothesised that HvAP2 also
196 controls floral development by modulating target gene(s) expression. We selected candidate
197 *HvMADS-box* genes based on their predicted function, AP2-like binding motifs in their regulatory
198 regions, expression in relevant tissues and whether they were differentially expressed in our earlier
199 *Zeo1.b* microarray study (Fig. S6, S7; Table S5; Patil *et al.*, 2019). Our top candidate was *HvMADS1*
200 (HORVU4Hr1G067680.2). The *HvMADS1* rice orthologue in rice, *OsMADS1/ LEAFY HULL STERILE*
201 (*LHS1*) promotes lemma and lodicule identity and differentiation, transforms glumes into lemmas
202 when overexpressed and causes glume-like lemmas and elongated bract-like lodicules when down-
203 regulated (Prasad *et al.*, 2001, 2005). *HvMADS1* is expressed in differentiating spikelets, lemmas and
204 lodicules (Fig. S7) and co-expressed with *HvAP2* in RNA-seq datasets of spikelet development (Digel
205 *et al.*, 2015). We sampled developing spikes in Bowman, *gigas1.a* and *Zeo1.b* genotypes, normalising
206 expression to Bowman. *HvMADS1* expression increased in all genotypes between WD3.5 to WD4.0,
207 suggesting this temporal pattern is independent from HvAP2. Overall, *HvMADS1* transcripts were
208 little changed in *gigas1.a*, so factors other than HvAP2 likely contribute to *HvMADS1* expression in
209 *gigas1.a*. However, we detected increased *HvMADS1* expression in *Zeo1.b* WD4 and WD5.5 spikes
210 compared to Bowman (Fig. 3D; Fig. S8). In situ hybridisation with an antisense *HvMADS1* probe gave
211 a strong signal in young and older *Zeo1.b* spikelets compared to Bowman, especially within
212 developing glumes, lemma/palea, lodicule and stamen primordia (Fig. 3E,F). These data support that
213 ectopic HvAP2 promotes *HvMADS1* expression, potentially explaining the glume to lemma
214 transformations in *Zeo1.b*.

215 Other potential HvAP2 targets include *HvMADS2* (HORVU3Hr1G091000.8) and *HvMADS4*
216 (HORVU1Hr1G063620.2), whose orthologue, the 'B' class *PISTILLATA* (*PI*) gene, is a direct negative
217 target of Arabidopsis AtAP2 (Krogan et al., 2012). *HvMADS2* expression increased in *gigas1.a* at
218 WD5, and *HvMADS4* expression showed no HvAP2-dependent differences (Fig S8). We also
219 examined the expression of *HvMADS3* (HORVU3Hr1G026650.1) and *HvMADS58*

(HORVU1Hr1G029220.1), two *AGAMOUS-like* genes whose orthologues in Arabidopsis are direct targets of AtAP2 (Zhao *et al.*, 2007; Yant *et al.*, 2010; Ripoll *et al.*, 2011). *HvMADS3* was lower in *Zeo1.b* at WD5 and *HvMADS58* expression was lower in *gigas1.a* at WD4 compared to Bowman and *Zeo1.b* (Fig. 3D; Fig. S8). Reduced *HvMADS58* expression could contribute to *gigas1.a* lodicule and pistil phenotypes, since *OsMADS58* is essential for carpel and lodicule identity in rice (Yamaguchi *et al.*, 2006; Dreni *et al.*, 2011) while *AtSHP1* orthologue promotes stigmatic papillae formation in Arabidopsis (Colombo et al., 2010). Altogether, our comparative gene expression analyses link HvAP2-dependent changes in floral organ development with and specific *MADS-box* gene mis-expression. Whether this relationship is direct is unknown.

HvAP2 promotes maternal tissue degeneration during caryopsis development

To learn when HvAP2 alters grain parameters, we tracked changes in pre-anthesis ovary and caryopsis dimensions at days post anthesis (DPA). Depth was measured along the dorsal:ventral axis. Compared to Bowman, *gigas1.a* ovaries were 12% longer, 20% wider, 24% deeper (all $p<0.001$) and 70% lighter ($p<0.01$; Fig 4A,B; Fig S9; Table S6). Post-fertilisation, *gigas1.a* caryopses became 36% and 55% longer at 10 and 30 DPA respectively ($p<0.001$), and remained narrower during most growth ($p<0.05$; Fig 4A,B; Table S6). Caryopses in *gigas1.a* were 9–16% shallower 15–25 DPA ($p<0.05$) and 10-50% lighter ($p<0.01$) compared to Bowman until final stages (Fig S9; Table S6). Pre-anthesis, *Zeo1.b* ovaries were 16% deeper ($p<0.001$), 6% shorter ($p<0.001$) and 36% lighter ($p<0.01$) and following fertilisation, *Zeo1.b* caryopses 5 DPA were 30% shorter ($p<0.05$) and afterwards showed no clear length or depth trend but became progressively heavier (Fig 4A; Table S6). *Zeo1.b* caryopses were 20% wider ($p<0.001$), and 10% heavier ($p<0.01$) than Bowman by 30 DPA (Table S6). Overall, HvAP2 activity positively correlated with wider and heavier grain during grain fill while loss of HvAP2 function lengthened and narrowed grain.

We examined transverse sections of developing caryopses to explore potential causes of HvAP2-dependent differences. Bowman caryopses showed a dumbbell-shaped embryo sac with dorsal indentations at 5 DPA, while the *gigas1.a* embryo sac was rectangular-shaped and the *Zeo1.b* embryo uniformly oval (Fig. 4C). Variation in embryo sac shape correlated with differences in the lateral and dorsal mesocarp provascular strands, structures that supply nutrients to the pericarp before degenerating (Fisher, 1990). Caryopses from *gigas1.a* displayed provascular strands, Bowman showed remnants of provascular strands and *Zeo1.b* lacked any trace of provascular strands (Fig. 4C), suggesting that HvAP2 accelerates provascular degeneration, potentially influencing the shape of the expanding embryo sac. The nucellar projection, a specialised structure that differentiates from the nucellus, also differed amongst alleles. Flanked by a pigment strand and vascular bundle, the nucellar projection transports nutrients from maternal to filial tissues before undergoing programmed cell death (PCD), leaving a large cavity (Radchuk *et al.*, 2006; Thiel *et al.*, 2008; Dominguez & Cejudo, 2014; Lu & Magnani, 2018). At 10 DPA, nucellar projection degeneration was least noticeable in *gigas1.a* while *Zeo1.b* showed more break-down compared to Bowman, with corresponding differences in cavity size (Fig. 4D). Thus, HvAP2 may promote break-down of nucellar tissues. We also detected differences in the integuments across *HvAP2* alleles. Grass ovules have outer and inner integuments, and the outer integument degrading rapidly following fertilisation (Kellogg, 2015). At 5 DPA, Bowman and *Zeo1.b* showed the two-layered inner integument while *gigas1.a* had inner integuments plus multiple layers of enlarged integument-like cells which may be a non-degraded outer integument (Fig. 4E). By 10 DPA, the inner integuments of Bowman and *Zeo1.b* were crushed, along with most of the nucellar epidermis, to form the seed coat (Fig. 4F). At 10 DPA, the inner integuments and nucellar epidermis of *gigas1.a* also compressed into the seed coat, but the extra integument-like layers persisted, separated from the pericarp by a prominent cuticle (Fig. 4F). Altogether, loss of HvAP2 function inhibited or profoundly delayed the degradation of multiple maternal tissues while gain of HvAP2 function promoted the degradation of multiple

maternal tissues. We propose that *HvAP2* is a critical negative regulator of maternal tissue growth and survival during grain development.

We asked whether *HvAP2* expression correlated with its proposed roles in the grain. *HvAP2* transcripts localise to lodicule primordia as well as the lemma and glume (Nair *et al.*, 2010; Anwar *et al.*, 2018) but the *HvAP2* expression pattern in grain has yet to be reported. We detected *HvAP2* mRNA in the lemma and pre-anthesis ovary, and concentrated expression in the vascular bundle, pigment strand and nucellar projection at 2 DPA (Fig. 4G; Fig. S10). By 5 and 10 DPA, *HvAP2* transcripts persisted in remaining nucellar tissues, seed coat and pericarp (Fig. 4G). Taken together, *HvAP2* transcripts accumulate in tissues altered due to *HvAP2* allelic variation.

We used qPCR to examine expression levels of potential downstream genes in the developing grain. We were particularly interested in *HvMADS29* (HORVU6Hr1G032220), a gene almost exclusively expressed in young grain (Fig. S7) and the orthologue of a B-sister gene (the closest relatives of B-class genes) in rice called *OsMADS29*. Down-regulation of *OsMADS29* in rice inhibits degradation of all maternal tissues, including the nucellus and nucellar projection, leading to shrunken seeds (Yin & Xue, 2012; Yang *et al.*, 2012). *HvMADS29* expression was reduced to 37% of the Bowman level in *gigas1.a* grain at 5 DPA (Fig. 4H). Although the 'C' class *HvMADS3* and *HvMADS58* are also highly expressed in grain (Fig. S7, S11), neither were differentially regulated in *gigas1.a* 5 DPA grain (Fig. S12). Jasmonate (JA) positively regulates nucellus programmed cell death (PCD(in tomato (Schubert *et al.*, 2019) and is associated with PCD in barley grain (Sreenivasulu *et al.*, 2006). Our previous work suggested that HvAP2 promotes JA-associated gene expression to suppress growth (Patil *et al.*, 2019). Here, we show that transcripts encoding two jasmonate-induced proteins, JIP23 and JIP60, expressed during barley grain development (Fig. S7, S11), were strongly downregulated in *gigas1.a* caryopses at 5DPA compared to Bowman (Fig. 4H). In sum, lower levels of *HvMADS29* and *JIP* transcripts agree with the reduced maternal PCD in *gigas1.a* and consistent with being putative targets of direct or indirect regulation by HvAP2.

294

295 **HvMADS29 contributes to the formation of nucellus projection and vascular bundle**

296 To assess the relationship between HvAP2 and HvMADS29 in greater detail, we addressed the role of
297 HvMADS29 in caryopsis development. RNA-seq data from unfertilised pistils and developing grain
298 staged by days after pollination (DAP) (Aubert *et al.*, 2018) indicated that *HvMADS29* expression
299 increases during pre-anthesis stages before peaking around 9 DAP and subsequently decreasing
300 during grain development (Fig 5A). Prior to fertilisation, *HvMADS29* expression overlaps with *HvAP2*
301 (in addition to *HvMADS1*, *HvMADS3* and *HvMADS58*), although *HvMADS29* is subsequently
302 maintained during grain development when *HvAP2* levels decrease (Fig S11). *In situ* hybridisation
303 showed *HvMADS29* expression in the developing ovule, predominantly in the nucellus, integuments
304 and embryo sac (Fig S11), in agreement with previous microarrays showing *HvMADS29* expression in
305 maternal tissues (Thiel *et al.*, 2008). After fertilisation, *HvMADS29* showed weak expression in the
306 integuments and strong signals in the vascular bundles overlying the nucellar projection and in
307 peripheral vascular bundles (Fig. 5B), overlapping with the pattern observed for *HvAP2*.

308 To directly demonstrate the importance of *HvMADS29* for caryopsis development, we edited the
309 *HvMADS29* gene using the CRISPR/Cas9 system (Ma *et al.*, 2015). Screening of 25 T0 transformants
310 in Golden Promise revealed five lines (*hvmads29*) with a one bp deletion in *HvMADS29*, leading to a
311 frame shift, early stop codon, and predicted complete loss of function (Fig. 5C). Caryopses of
312 *hvmads29* were malformed and shrivelled compared to Golden Promise with differences in ovule
313 development already evident at anthesis (Fig. 5D, Fig S12). In particular, the two layers of inner
314 integument cells showed similar morphology to Golden Promise but with an overall misshapen
315 structure, possibly due to reduced nucellus growth. In addition, the outer integument cells in
316 *hvmads29* were abnormally enlarged and occasionally exhibited three cell layers rather than the two
317 cell layers detected in Golden Promise (Fig S13). Defects in caryopsis development were particularly
318 obvious at 5 DPA, when *hvmads29* grain appeared thinner and unfilled, suggesting that defective

transport tissues including the nucellar projection and vascular bundle (Fig. 5E). Transverse sections of developing caryopses revealed that 5 DPA Golden Promise contained a well-developed nucellar projection, and a vascular bundle from the ventral pericarp joining the nucellar projection (Fig. 5F). Notably, the phloem cells intensely stained by calcofluor white highlighted the vascular bundle in a semi-circle pattern. By 10 DPA, the nucellar projection increased in size and differentiated various cell types. In *hvmads29*, the nucellus failed to degrade, the nucellar projection did not differentiate, no transport tissue was formed and the vascular bundle was shrunken with fewer phloem fibres, compared with wild type (Fig. 5F). Importantly, *hvmads29* mutants failed to produce endosperm or viable seed. Collectively, the putative *hvmads29-2* null allele shows several tissue-specific defects similar to *gigas1.a* in terms of defective integument development and an under-developed nucellar projection. Along with the qPCR, RNAseq and *in situ* data, this provides additional evidence that *HvAP2* and *HvMADS29* both influence the development and differentiation of transport tissues, particularly in the nucellar projection. We speculate that HvAP2 may contribute to upstream control of *HvMADS29* expression, but this relationship remains to be tested.

HvAP2 interacts with HvBOP2 to control lodicule identity and grain length

While HvMADS29 and HvMADS1 may mediate some HvAP2 functions, we know little other factors interacting with *HvAP2* beyond miR172. Deletion of the transcription factor-encoding gene *HvBLADE-ON-PETIOLE2* (*HvBOP2*) in *laxatum.a* (*lax.a*, BW419) causes lax spikes, elongated, narrow paleas and lemmas, an impaired lemma-awn boundary, skinny grain, and transforms lodicules into stamens, leading to open-flowering (Jost *et al.*, 2016;Fig. 6A–I). We noted that *lax.a* also develops needle-like glumes, elongated, narrow ovaries and shorter lemma awns ($p<0.04$; Fig. 6C–D; Fig. S13). Since *lax.a* and *gigas1.a* share some phenotypes, we speculated that *HvAP2* and *HvBOP2* may interact. To explore this hypothesis, we generated *gigas1.a lax.a* and *Zeo1.b lax.a* double mutants. Most double mutant phenotypes suggested independent, additive roles of HvAP2 and HvBOP2. The *gigas1.a lax.a* double mutant displayed more extreme open-flowering than either parent, needle-

like *lax.a* glumes equivalent in length to *gigas1.a* (p=0.86), lemma length equivalent to *lax.a* (p=0.31) and lemma awns shorter than either parent (p<0.02), and with a more impaired awn-lemma boundary, as well as narrow ovaries lacking stigmatic papillae and extremely narrow grain (p≤0.001; Fig. 6A-I; Fig S13, S14; Table S7). *Zeo1.b lax.a* lemmas had shorter awns (p≤0.001) similar to *Zeo1.b*, and defective awn-lemma boundaries similar to *lax.a*. (Fig. 6E,F; Fig. S13; Table S7). The *Zeo1.b lax.a* mutant also retained *Zeo1.b* glume to lemma transformation but these organs were extremely thin with longer awns, indicating that loss of *HvBOP2* influences lemma morphology regardless of position, (p≤0.001; Fig. 6C,D; Table S7). Grain of *gigas1.a lax.a* showed the same narrow grain as *lax.a* (p=0.26; Fig 6I; Fig S14). Interestingly, the *Zeo1.b lax.a* mutant showed both *lax.a* elongated lemmas while also displaying *Zeo1.b* shortened grain (p<0.05; Fig 6I,J; Fig S14), suggesting that these two traits can be uncoupled. However, *Zeo1.b lax.a* double mutants also showed striking epistasis in other features. Double mutants showed *Zeo1.b*-like spike density (p≤0.001) and a recovery of lodicule identity with *Zeo1.b*-like morphology (Fig. 6A,B,G,H; Fig. S14, S15, Table S6), while *Zeo1.b*/+ *lax.a* plants showed lodicule/stamen mosaic-like structures (Fig. S15). Thus, we propose that *HvAP2* may act downstream of HvBOP2 in the control of spike density, grain length and lodicule identity. To explore the molecular nature of this interaction, we analysed *HvAP2* and *Hvmir172* expression in Bowman and *lax.a* mutant plants. We detected no difference in HvAP2 mRNA levels in entire seedlings at two weeks after planting or developing spikes; however, However, we detected slightly elevated levels of *Hvmir172* in *lax.a* as well as lowered levels in *Zeo1.b*, suggesting that HvAP2 suppresses levels of *HvmiR172* and that HvBOP2 may enhance *HvmiR172* expression (Fig S16).

DISCUSSION

Cereal yield depends upon multiple factors including floret number, coordinated growth of floral organs, fertilisation and relocation of maternal nutrients to the developing seed (Brinton *et al.*, 2017; Wilkinson *et al.*, 2019; Sakuma & Schnurbusch, 2020; Ren *et al.*, 2020; Paul *et al.*, 2020). Targeted

modification of individual factors is challenging because they typically have both direct and indirect impacts on grain size, number and quality (Wang *et al.*, 2012; Xie *et al.*, 2015; Si *et al.*, 2016; Bull *et al.*, 2017; Wilkinson *et al.*, 2018; Li *et al.*, 2019). One way to dissect pleiotropic effects is to characterise key regulatory modules and genes that contribute to tissue-specificity. Here we show via analysis of the *gigas1.a*, *hvap2* and *Zeo1.b* mutants that HvAP2 is a major regulator of barley reproductive development that influences tissue-specific factors in the flower and seed (Fig 6).

HvAP2 promotes and accelerates the transition to floret identity

Effects on the perianth from gain and loss of *HvAP2* function alleles (Fig1,2) and restored lodicule identity in *Zeo1.b lax.a* (Fig 6) show that HvAP2 promotes perianth organ identity and defines the outer perianth boundary, suggesting that HvAP2 participates in the commitment to floret fate. Barley lacking *HvmiR172* expression and wheat with strong overexpression of *TaAP2L5* shows a complete conversion of glumes to florets (Brown & Bregitzer, 2011; Debernardi *et al.*, 2017; Greenwood *et al.*, 2017; Song *et al.*, 2019). Since homeotic lemmas in *Zeo1.b* did not enclose floret organs, we suggest that gain of HvAP2 function in *Zeo1.b* is insufficient for ectopic florets and instead gives rise to 'sterile lemmas' - intermediate organs normally found in cultivated rice, and in wheat with moderate overexpression of *TaAP2L5* (Debernardi *et al.*, 2017; Greenwood *et al.*, 2017; Song *et al.*, 2019). Our interpretation supports previous suggestions that glumes, sterile lemmas and lemmas develop on an ontogenetic gradient which determines their axillary meristem's fate, from glumes subtending spikelet meristems, to empty sterile lemmas, and finally to fertile lemmas subtending floret meristems (Malcomber *et al.*, 2006; Lee *et al.*, 2007; Chuck *et al.*, 2008; Lee & An, 2012; Song *et al.*, 2019; Debernardi *et al.*, 2020). We propose that the gradient shifts towards fertile lemma identity with increasing AP2L function, making *AP2L* genes master regulators of floret establishment in grasses.

393 Control of floral fate by *AP2L*s likely involves the *LHS1*-like subclade of the 'E' class *SEPALLATA* genes
394 considered central for the evolution of the floret-bearing grass spikelet (Malcomber & Kellogg,
395 2004). The rice APL2s SNB and IDS1 promote the expression of the *LHS1*-like *OsMADS1* which
396 confers perianth organ identity and accelerates the transition from spikelet to floret meristem fate
397 (Jeon *et al.*, 2000; Prasad *et al.*, 2001, 2005; Ohmori *et al.*, 2009; Lee & An, 2012; Khanday *et al.*,
398 2013; Dai *et al.*, 2016). HvAP2-dependent changes in *HvMADS1* expression (Fig 3D,F; Fig S5B),
399 suggest that HvMADS1 also promotes perianth and floret identity in barley. Elevated JA-signalling in
400 *Zeo1.b* (Patil *et al.*, 2019) may also contribute to HvAP2 regulation of *HvMADS1* since JA-signalling
401 upregulates *OsMADS1* expression in rice (You *et al.*, 2019). OsMADS1 inhibits *miR172* accumulation
402 and possibly directly regulates *AP2L*s (Khanday *et al.*, 2016; Dai *et al.*, 2016). We propose that
403 *HvMADS1* and *HvAP2* co-expression (Digel et al., 2015) and our data showing HvAP2-responsive
404 *HvMADS1* expression, reflect positive feedback which may coordinate identity switches and
405 hormone signalling to ensure a sharp transition from spikelet to floret fate. However, since
406 substantial *HvMADS1* levels persist in *gigas1.a* (Fig. 3D), factors besides HvAP2 must also upregulate
407 *HvMADS1* expression.

408

409 **HvAP2 promotes lodicule identity**

410 AP2 was first described in Arabidopsis as a class 'A' gene conferring sepal and petal identity
411 (Bowman *et al.*, 1989, 1991; Kunst *et al.*, 1989; Drews *et al.*, 1991). Weak *ap2* alleles develop
412 stamenoid petals and stronger *ap2* alleles show carpel-like transformation in the sepal and petal
413 whorl, phenotypes associated with loss of 'B' and 'E' class function and expanded 'C' class function
414 (Kunst *et al.*, 1989; Drews *et al.*, 1991; Jack *et al.*, 1992; Modrusan *et al.*, 1994; Goto & Meyerowitz,
415 1994). In wheat, loss of both TaAPL2 and TaAPL5 function leads to carpel-like structures on lodicules,
416 consistent with increased 'C' class *MADS3/ MADS58* (*TaAG1/ TaAG2*) expression and reduced 'B'
417 class gene expression at WD3.5–WD4.25 stages (Debernardi *et al.*, 2020). We did not observe

carpelloidy in *gigas1.a* or *hvap2-2* lodicules, which instead showed bract and filament-like transformations (Fig 1J-L; Fig. 2F–H). This may reflect reduced HvAP2 activation of *HvMADS1*, as SNB/OsIDS1-dependent expression of *OsMADS1* is important for lodicule formation development (Jeon *et al.*, 2000; Prasad *et al.*, 2001, 2005; Lee & An, 2012), rather than HvAP2 regulation of B or C class genes. However, *Zeo1.b* WD5.5 spikelets showed reduced *HvMADS3* mRNA abundance (Fig S8). In rice, ectopic expression of *OsMADS3* converted lodicules to stamens (Kyozuka & Shimamoto, 2002), an identical phenotype to *lax.a* (Jost et al., 2016; Fig 6G). Thus, *Zeo1.b* dependent reductions in *HvMADS3* expression may help suppress homeotic stamen identity in *Zeo1.b lax.a* lodicules (Fig 6G). Thus, we propose that HvAP2 may control lodicule differentiation through regulating both 'C' and 'E' class genes. Nonetheless, lodicules in *gigas1.a* or *hvap2-2* usually retained lodicule features, so other genes must confer lodicule identity either along with *HvAP2* or when *HvAP2* function is impaired, consistent with redundant control of lodicule identity amongst wheat *AP2Ls* (Debernardi *et al.*, 2020). In Arabidopsis, AtBOP promotes AtAP2 function via the miR172-AP2 network (Khan et al., 2015). While we did not detect changes in *HvAP2* expression in *lax.a*, we speculate HvBOP2 could regulate HvAP2 at a protein level or that HvBOP2 may promote the function of other miR172-regulated *HvAP2L* genes to regulate lodicule identity.

HvAP2 elongates hulls and caryopses

Hulls are proposed to physically limit grain size in rice (Li & Li, 2016; Li *et al.*, 2019) and multiple rice grain size QTL control hull cell number and/or expansion (Song *et al.* 2007; Wang *et al.* 2012; Zhang *et al.* 2012; Si *et al.* 2016; Ren *et al.* 2016, 2018; Lyu *et al.* 2020; Ruan *et al.* 2020). Here, we found that hulls and grain in *gigas1.a* and *hvap2-2* equally elongated (Fig 1C,D,L-N; Fig 2D–E; Fig S4), suggesting that HvAP2 limits both hull and grain length. Interestingly, the mechanism differs between these tissues, with HvAP2-dependent repression of cell expansion underlying changes in lemma length, while HvAP2 is required to suppress both cell length and number in the pericarp.

443 Caryopses in *gigas1.a* extended longer than Bowman at 10 DPA, corresponding with the timing of
444 pericarp cell expansion in barley (Radchuk *et al.*, 2011). As pericarp cell number and length were
445 increased in *gigas1.a*, HvAP2 could limit this final cell longitudinal expansion event as well as earlier
446 proliferation, similar to its role in the internode (Patil *et al.*, 2019). HvAP2's role in ovary wall cell
447 length control appears conserved in grasses, where the rice *SNB* shortens both hull cell length and
448 pericarp epidermis cell length (Jiang *et al.*, 2019; Ma *et al.*, 2019), as well as in Arabidopsis where
449 miR172-resistant AP2 represses cell expansion in the replum valves (Ripoll et al., 2015). However,
450 while multiple genes, including *HvAP2*, may modulate grain length by influencing hull length, how
451 the hull mechanistically limits caryopsis growth is largely unexplained. For instance, do changes in
452 grain length occur in direct response to the hull, such as surface-surface contact and/or mechanical
453 pressure? Uncoupling of hull from grain length in the double mutant *Zeo1.b lax.a* mutant suggests
454 that HvAP2 and HvBOP2 may be key nodes in this communication. Learning the identity of putative
455 hull "signals" and how they might synchronise caryopsis development with hull proportions would
456 be a major advance in our understanding of the control of cereal grain size.

457

458 **HvAP2 and maternal degradation transitions**

459 While increased grain length can lead to heavier grain (Zhang *et al.*, 2012; Brinton *et al.*, 2017),
460 thousand grain weight increased only by 7% in *gigas1.a* since its grain in narrower and shallower (Fig
461 1; Fig S2; Fig 4; Fig S8). Our data links HvAP2-dependent variation in grain width and depth to an
462 altered balance between maternal versus filial growth and survival. Most strikingly, multiple
463 maternal tissues in *gigas1.a* show defective and/or delayed degradation (Fig 4) which may reduce
464 remobilisation of nutrients and/or space to enlarge, both considered critical for endosperm growth
465 (Radchuk *et al.*, 2006; Thiel *et al.*, 2008; Dominguez & Cejudo, 2014; Wilkinson *et al.*, 2019).
466 Impaired maternal elimination correlates with defective endosperm development across plants
467 (Radchuk *et al.*, 2011; Yin & Xue, 2012; Dominguez & Cejudo, 2014; Xu *et al.*, 2016), with nucellar

468 degradation playing a major role in promoting endosperm growth (Lu & Magnani, 2018). We show
469 here that *HvMADS29* expression is significantly reduced in *gigas1.a* (Fig 4H) and demonstrate for the
470 first time in temperate cereals that *MADS29* function is essential for nucellar differentiation and
471 degradation, control of integument growth and endosperm development. We propose that HvAP2
472 controls grain width and weight in part by influencing the rate of maternal degradation via *MADS29*-
473 driven processes, suggesting that coordination of filial endosperm expansion with the maternal
474 tissue degradation and differentiation is at least partially under phase change miR172/AP2 control.
475 In rice and Arabidopsis, the B-sister genes *OsMADS29* and *TRANSPARENT TESTA16* (*TT16*),
476 respectively, promote the degeneration of nucellar and other maternal tissues in response to auxin
477 produced from the endosperm following fertilisation (Yin & Xue, 2012; Yang *et al.*, 2012; Nayar *et al.*,
478 2013; Xu *et al.*, 2016; Lu & Magnani, 2018). Whether HvAP2 directly regulates HvMADS29 and/or
479 other activators of nucellar elimination in response to filial signals remains a pressing question.

480 In Arabidopsis, signals from the endosperm transform integuments into the seed coat (Figueiredo *et*
481 *al.*, 2016), a process sustained by mechanical pressure from the expanding endosperm (Creff *et al.*,
482 2015). This in turn limits endosperm growth (Garcia et al., 2005), highlighting a developmental
483 interdependency which may underlie *ap2* mutant seed phenotypes. AtAP2 appears necessary to
484 restrict integument cell expansion, promote seed coat epidermal differentiation, accelerate
485 endosperm cellularisation and constrain endosperm cell expansion, roles linked to limits on seed
486 weight and size, embryo size, storage protein accumulation and sugar metabolism (Jofuku *et al.*,
487 1994; Ohto *et al.*, 2005, 2009). Our data suggest that HvAP2 limits integument number in barley,
488 potentially by promoting the degradation of the outer integument, showcasing a role for an *AP2L*
489 gene in cereal integument development, a role which may relate to regulation of *HvMADS29*, since
490 anthesis-stage *hvmads29* ovules showed abnormally enlarged cells in disorganised integument
491 layers. In Arabidopsis, TT16 coordinates communication between the integuments and endosperm
492 (Xu *et al.*, 2016), promotes inner integument flavonoid deposition and differentiation (Nesi *et al.*,
493 2002) and controls outer integument thickness (Fiume *et al.*, 2017) while a recently duplicated B-

494 sister gene, *GORDITA* (*GOA*) contributes to outer integument differentiation (Prasad *et al.*, 2010).
495 Although *HvMADS29* is clearly not relevant to all functions of HvAP2, tissue-specific regulation of
496 one or more of the three barley B-sister genes (Yang *et al*., 2012) by HvAP2 may explain the darker
497 seeds and persistence of the outer integuments in *gigas1.a*, in addition to alterations in the rate of
498 nucellar degradation. Increased proanthocyanidins in the seed coat of barley are associated with
499 increased dormancy (Himi *et al.*, 2012). We observed that germination of *gigas1.a* grain was less
500 efficient compared to wild type, suggesting that HvAP2 may influence seed germination through its
501 effects on the seed coat.

502

503 **Spikelet and grain traits and domestication**

504 Changes in lemma and palea dimensions control the overall shape of the floret, influencing final
505 grain size while lodicule size and swelling leads to open flowering. Similar to *gigas1.a*, wild barley
506 (*Hordeum spontaneum*) shows elongated lance-shaped hulls and open flowering compared to the
507 wedge-shaped form of cultivated barley (Abdel-Ghani *et al.*, 2004; Clayton, 2006). While wild barley
508 populations show large variation in seed size (Chen *et al.*, 2004), cultivated barley grain tends to be
509 shorter, wider and heavier (Fuller, 2007; Hughes *et al.*, 2019) with more uniform germination (Fuller
510 & Allaby, 2018). Our data suggests that HvAP2 controls multiple traits which differ between wild and
511 cultivated barley. In wheat and rice, selection of allelic variation in *AP2L* genes was associated with
512 improved grain traits (Xie *et al.*, 2018; Jiang *et al.*, 2019). It is tempting to speculate that changes in
513 HvAP2 function and/or *HvMADS* regulation contributed to selection for changes in spikelet and grain
514 during barley cultivation.

515

516 **MATERIALS AND METHODS**

517 **Plant material, growth conditions and BWNIL genotyping**

Parent cultivars and mutant germplasm are listed in Table S1. Plants were grown in the glasshouse under 16 hours light and day/night temperatures of 18/15°C. Plants were grown in plastic pots filled with universal compost (1200l of peat, 100l of sand, 2.5kg of magnesium limestone, 2.5kg of calcium limestone, 1.5kg of Osmocote® Start (11N-4.8P-14.1K+1.2Mg+TE), 3.5kg of Osmocote® Exact Standard 3-4M (16N-3.9P-10K+1.2Mg+TE), 0.5kg of Celcote, 100l of Perlite, 390g of Intercept insecticide (active ingredient: imidacloprid). Golden Promise and *hvmads29* plants were grown in controlled environment reach-in chambers in The Plant Accelerator, the University of Adelaide, under the same conditions as plant materials grown in the UK. gDNA from the *gigas1.a* (BW381), Bowman and Golden Melon were genotyped using the Barley 50K SNP chip (Bayer et al., 2017).

Phenotyping, microscopy and in situ hybridisation

Whole plant phenotypic measurements were taken from mature plants. Spikelet length was measured from the base of the spikelet to the lemma-awn boundary on the 4th spikelet from the base of the spike. Awns were measured from awn tip to the top of the glume or lemma body. Spike length was the length from the collar node to the top of the rachis (spike axis). Spikelet width was measured at the widest part of the lemma. Culm height was measured from the top of the soil to the collar at the base of the spike. Mature and developing Bowman, *Zeo1.b* and *gigas1.a* spikes were harvested at 21, 23, 25, 30 and 35 days after germination, their length recorded and stages assigned based on (Waddington *et al.*, 1983); Table S7). Scanning electron microscopy was performed as described (Houston et al., 2012). Mature grain width and length were analysed using MARVIN-Universal (GTA Sensorik GmbH). Developing caryopses (n=5 independent replicate grains per genotype) were sampled on their respective DPA. For Golden Promise and *hvmads29* samples, caryopses were collected at anthesis, 5 and 10 DPA, photographed by stereo microscope (Leica, MZ FLIII) or fixed in FAA solution, dehydrated in an ethanol series and embedded in Technovit 7100 resin (Kulzer Technique). Transverse 1.5 µm sections were stained with Calcofluor White (Sigma-Aldrich)

or 1% toluidine blue. Sections were photographed using a Zeiss AxioImager M2, for cell wall (excitation, 335–383 nm; emission, 420–470 nm) and auto fluorescence (excitation, 538–562 nm; emission, 570–640 nm).

HvAP2 in situ hybridization was performed as described previously (Hands *et al.*, 2012) and *HvMADS29 in situ* hybridisation was performed automatically using an InsituPro VSi robot (Intavis), following a standard protocol (Javelle *et al.*, 2011). 2225bp and 319bp cDNA fragments were amplified from Bw cDNA using primers fused to the T7 promoter as a template for *HvAP2* and *HvMADS1* in situ probes, respectively (Table S9). Digoxigenin-labeled antisense and sense probes were transcribed using T7 polymerase (ThermoFisher) according to the manufacturer's instructions.

CRISPR/Cas9 vector cloning

CRISPR/Cas9 technology was used to generate mutations in *HvAP2* at the University of Dundee (Garcia-Gimenez *et al.*, 2020). Two guide RNAs (gRNAs) were designed (Table S9) using the Broad Institute sgRNA Designer and the Zhao Bioinformatics Laboratory pssRNAit (Noble Foundation). Each gRNA was cloned into pC95-gRNA entry vector downstream of the rice small nuclear RNA (snRNA) U6 promoter (OsU6p) by Gibson Assembly®. Each sgRNA cassette was then released and inserted into pBract214m-bcoCas9-HSPT expression vector which contains a barley codon optimised Cas9 (bcoCas9) under the control of maize ubiquitin promoter and Arabidopsis heat shock protein 18.2 terminator. The resultant construct was transformed by electroporation into Agrobacterium strain AGL1 containing replication helper pSoup. Transformed Agrobacterium clones from each CRISPR construct were combined and co-transformed into Golden Promise immature embryos (Bartlett *et al.*, 2008) in the FUNGEN facility at The James Hutton Institute, Dundee, UK. Transgenic plants containing CRISPR constructs were regenerated under hygromycin selection. Of the 174 T0 plants, 143 were transformed with a single gRNA from 35 separate calli and 31 plants transformed with the two gRNAs from 12 different calli. No mutations were found in the single gRNA transformation lines

and one was detected in the double transformation lines. We examined 16 individuals from 18 T1 lines (originating from 10 different T0 calli) which still contained the *Cas9* gene. We detected three homozygous mutations in these T1, including a 39bp deletion (*hvap2-1*) in nine different lines from three different calli and a 40bp deletion (*hvap2-2*) in four lines from two different calli. In the T2 generation, following segregation of Cas9, *hvap2-1*, *hvap2-2* and Golden Promise were phenotyped (n = 8 per genotype).

We used a monocot-optimised CRISPR/Cas9 system (Ma *et al.*, 2015) to create the *hvmads29* mutant at the University of Adelaide. The selected target of *HvMADS29* was sequenced before the sgRNA expression cassette was amplified from vector pYLsgRNA-OsU6a and cloned into a binary vector pYLCRISPR/Cas9Pubi-H using BsaI sites as described (Ma *et al.*, 2015). The CRISPR construct was transformed into Golden Promise by *A. tumefaciens* AGL1 as previously described (Harwood *et al.*, 2009). A total of 25 T0 transformants were analysed in greater detail.

CRISPR/Cas9 screening and genotyping

For *HvAP2* CRISPR lines, genotyping conditions are described in Methods S1 and primers listed in Table S10. Genomic DNA (gDNA) was isolated from young leaf tissue using the Qiagen DNA easy plant mini kit. Cas9 was detected using Cas9 primers. A region spanning 1kb around the gRNA target region was amplified using external primers followed by a nested PCR using FAM-labelled internal primers. This product was analysed using a capillary sequencer, and genotypes were determined using GeneMapper® Software 5. Samples predicted to contain insertions and/or deletions (indels) were re-amplified without FAM-labelling and sequenced. T0 and T1 plants from *HvMADS29* CRISPR transformation events were genotyped using a Phire Plant Direct PCR Kit (Thermo Fisher Scientific) to amplify a 588bp fragment that was directly sequenced by Sanger sequencing (AGRF, Australia).

qRT-PCR

RNA extraction and qRT-PCR were performed as in (Patil et al., 2019) with the following modifications. RNA was isolated from entire spikes harvested at 23 days after sowing (DAS), 25 DAS, 30 DAS, 35 DAS and 40 DAS. cDNA was synthesised using ProtoScriptII kit (NEB) using random primers. The qPCR was normalised using RQ values calculated by the Pfaffl method 2^ (-ddCT) (Pfaffl, 2001). One replicate of Bowman at the earliest timepoint was normalised to 1.0 and each other sample replicates normalised to this value. We used *ACTIN2* (*HvACT2*) and *PROTODERMAL FACTOR7* (*HvPDF7*), as endogenous controls as in Patil et al (2019). SYBR Green Power Up (Thermofisher) kit was used to detect *HvJIP23*, *HvJIP60*, *HvmiR172* and *HvsnoR101* transcripts. Primers for qPCR are listed in Table S11.

Double mutant generation

Double mutants between *gigas1.a* or *Zeo1.b* with *lax.a* were generated by crossing. Double *Zeo1.b lax.a* and *Zeo1.b*/ + heterozygote *lax.a* mutants were isolated by screening a segregating *Zeo1.b*/*lax.a* F2 population which showed the expected ratio of double homozygotes of 1:16 (Table S12). An F3 population from a *Zeo1.b*/*lax.a* F2 individual was grown and segregated as expected. The *gigas1.a lax.a* F2 population was screened by genotyping with CAPS markers to isolate double mutants (Methods S1, Table S10).

Statistical analysis

Data were modelled in R 3.5.1 using an analysis of variance. Models were checked visually for normality in variance and any non-significant terms dropped from the model. Where only two genotypes were compared, and a two-tailed un-paired t-test was performed. Multiple genotypes

were compared using a Tukey honestly significant difference (HSD) test on the modelled data. Grain dimensions over time were analysed by ANOVA followed by a Dunn's post-hoc test.

ACKNOWLEDGEMENTS

This work was supported by Biological and Biotechnological Research Council (BBSRC) grant (BB/L001934/1) to S.M.M, and an Australian Research Council grant (DP180104092) to M.R.T. S.M.M. also acknowledges support from the University of Dundee and a Personal Research Fellowship from the Royal Society of Edinburgh. J.S. and K.H. acknowledge funding from the Scottish Government RESAS strategic research program. S.D. acknowledges support from the University of Leicester and from Natalie Allcock and Ania Straatman-Iwanowska in the Electron Microscopy Facility. M.R.T and X.Y. acknowledge technical support from Mr Chao Ma for operation of the *in situ* robot and plant maintenance. J.S. and L.P are supported by the BBSRC EASTBIO PhD program (grant number BB/J01446X/1). C.S. was supported by TETFUND Nigeria. M.E. is supported by a CARA Research Fellowship and by the University of Dundee. E.V.E and S.C. was supported by the ERASMUS+ programme and their home institutes, Hogeschool van Arnhem en Nijmegen and De Leijgraaf, respectively. A.B. is funded by the European Research Council (Shuffle Project ID: 669182).

REFERENCES

Aastrup S, Outtrup H, Erdal K. 1984. Location of the proanthocyanidins in the barley grain. *Carlsberg Research Communications* **49**: 105–109.

Abdel-Ghani AH, Parzies HK, Omary A, Geiger HH. 2004. Estimating the outcrossing rate of barley landraces and wild barley populations collected from ecologically different regions of Jordan. *Theoretical and Applied Genetics* **109**: 588–595.

Anwar N, Ohta M, Yazawa T, Sato Y, Li C, Tagiri A, Sakuma M, Nussbaumer T, Bregitzer P, Pourkheirandish M, *et al.* 2018. miR172 downregulates the translation of cleistogamy 1 in barley. *Annals of Botany* **122**: 251–265.

Arber A. 2010. *The Gramineae*. Cambridge: Cambridge University Press.

Aubert MK, Coventry S, Shirley NJ, Betts NS, Würschum T, Burton RA, Tucker MR. 2018. Differences in hydrolytic enzyme activity accompany natural variation in mature aleurone morphology in barley (Hordeum vulgare L.). *Scientific Reports* **8**: 11025.

Bartlett JG, Alves SC, Smedley M, Snape JW, Harwood WA. 2008. High-throughput Agrobacterium-

mediated barley transformation. *Plant Methods* **4**: 22.

Bayer MM, Rapazote-Flores P, Ganal M, Hedley PE, Macaulay M, Plieske J, Ramsay L, Russell J, Shaw PD, Thomas W, *et al.* 2017. Development and evaluation of a barley 50k iSelect SNP array. *Frontiers in Plant Science*.

Bowman JL, Smyth DR, Meyerowitz EM. 1989. Genes Directing Flower Development in Arabidopsis. *The Plant Cell* **1**: 37.

Bowman JL, Smyth DR, Meyerowitz EM. 1991. Genetic interactions among floral homeotic genes of Arabidopsis. *Development* **112**: 1 LP – 20.

Brinton J, Simmonds J, Minter F, Leverington-Waite M, Snape J, Uauy C. 2017. Increased pericarp cell length underlies a major quantitative trait locus for grain weight in hexaploid wheat. *New Phytologist* **215**: 1026–1038.

Brinton J, Uauy C. 2019. A reductionist approach to dissecting grain weight and yield in wheat. *Journal of Integrative Plant Biology* **61**: 337–358.

Brown RH, Bregitzer P. 2011. A Ds Insertional Mutant of a Barley miR172 Gene Results in Indeterminate Spikelet Development. *Crop Science* **51**: 1664–1672.

Bull H, Casao MC, Zwirek M, Flavell AJ, Thomas WTB, Guo W, Zhang R, Rapazote-Flores P, Kyriakidis S, Russell J, *et al.* 2017. Barley SIX-ROWED SPIKE3 encodes a putative Jumonji C-type H3K9me2/me3 demethylase that represses lateral spikelet fertility. *Nature Communications* **8**: 936.

Chen G, Suprunova T, Krugman T, Fahima T, Nevo E. 2004. Ecogeographic and genetic determinants of kernel weight and colour of wild barley (Hordeum spontaneum) populations in Israel. *Seed Science Research* **14**: 137–146.

Chuck G, Meeley R, Hake S. 2008. Floral meristem initiation and meristem cell fate are regulated by the maize AP2 genes ids1 and sid1. *Development* **135**: 3013–3019.

Clayton. 2006. http://www.kew.org/data/grasses-db/cite.htm. *Kew Database*.

Creff A, Brocard L, Ingram G. 2015. A mechanically sensitive cell layer regulates the physical properties of the Arabidopsis seed coat. *Nature Communications* **6**.

Dai Z, Wang J, Zhu M, Miao X, Shi Z. 2016. OsMADS1 Represses microRNA172 in Elongation of Palea/Lemma Development in Rice. *Frontiers in Plant Science* **7**: 1891.

Debernardi JM, Greenwood JR, Jean Finnegan E, Jernstedt J, Dubcovsky J. 2020. APETALA 2- like genes AP2L2 and Q specify lemma identity and axillary floral meristem development in wheat. *The Plant Journal* **101**: 171–187.

Debernardi JM, Lin H, Chuck G, Faris JD, Dubcovsky J. 2017. microRNA172 plays a crucial role in wheat spike morphogenesis and grain threshability. *Development* **144**: 1966–1975.

Digel B, Pankin A, von Korff M. 2015. Global Transcriptome Profiling of Developing Leaf and Shoot Apices Reveals Distinct Genetic and Environmental Control of Floral Transition and Inflorescence Development in Barley. *The Plant Cell* **27**: 2318–2334.

Dinh TT, Girke T, Liu X, Yant L, Schmid M, Chen X. 2012. The floral homeotic protein APETALA2 recognizes and acts through an AT-rich sequence element. *Development* **139**: 1978–1986.

Dominguez F, Cejudo FJ. 2014. Programmed cell death (PCD): an essential process of cereal seed development and germination. *Frontiers in Plant Science* **5**: 366.

Dreni L, Pilatone A, Yun D, Erreni S, Pajoro A, Caporali E, Zhang D, Kater MM. 2011. Functional

Analysis of All AGAMOUS Subfamily Members in Rice Reveals Their Roles in Reproductive Organ Identity Determination and Meristem Determinacy. *The Plant Cell* **23**: 2850–2863.

Drews GN, Bowman JL, Meyerowitz EM. **1991a**. Negative regulation of the Arabidopsis homeotic gene AGAMOUS by the APETALA2 product. *Cell* **65**: 991–1002.

Drews GN, Bowman JL, Meyerowitz EM. **1991b**. Negative regulation of the Arabidopsis homeotic gene AGAMOUS by the APETALA2 product. *Cell* **65**: 991–1002.

Druka A, Franckowiak J, Lundqvist U, Bonar N, Alexander J, Houston K, Radovic S, Shahinnia F, Vendramin V, Morgante M, *et al.* 2011. Genetic Dissection of Barley Morphology and Development. *Plant Physiology* **155**: 617–627.

Figueiredo DD, Batista RA, Roszak PJ, Hennig L, Köhler C. **2016**. Auxin production in the endosperm drives seed coat development in Arabidopsis. *eLife* **5**: e20542.

Fisher D. **1990**. Persistence of Non-Crease Protophloem Strands in the Developing Wheat Grain. *Functional Plant Biology* **17**: 223.

Fiume E, Coen O, Xu W, Lepiniec L, Magnani E. **2017**. Developmental patterning of sub-epidermal cells in the outer integument of Arabidopsis seeds (H Candela, Ed.). *PLOS ONE* **12**: e0188148.

Franckowiak J. 1995. Notes on linkage drag in Bowman backcross derived lines of spring barley. *Barley Genet Newsl* **24**: 63–70.

Fuller DQ. **2007**. Contrasting Patterns in Crop Domestication and Domestication Rates: Recent Archaeobotanical Insights from the Old World. *Annals of Botany* **100**: 903–924.

Fuller DQ, Allaby R. **2018**. Seed Dispersal and Crop Domestication: Shattering, Germination and Seasonality in Evolution Under Cultivation. *Annual Plant Reviews online*: 238–295.

Garcia-Gimenez G, Barakate A, Smith P, Stephens J, Khor SF, Doblin MS, Hao P, Bacic A, Fincher GB, Burton RA, *et al.* 2020. Targeted mutation of barley (1,3;1,4)-β-glucan synthases reveals complex relationships between the storage and cell wall polysaccharide content. *bioRxiv*: 2020.05.13.093146.

Goto K, Meyerowitz EM. **1994**. Function and regulation of the Arabidopsis floral homeotic gene PISTILLATA. *Genes and Development* **8**: 1548–1560.

Greenwood JR, Finnegan EJ, Watanabe N, Trevaskis B, Swain SM. **2017**. New alleles of the wheat domestication gene Q reveal multiple roles in growth and reproductive development. *Development* **144**: 1959–1965.

Hands P, Kourmpetli S, Sharples D, Harris RG, Drea S. **2012**. Analysis of grain characters in temperate grasses reveals distinctive patterns of endosperm organization associated with grain shape. *Journal of Experimental Botany*.

Harvey BL, Reinbergs E, Somaroo BH. **1968**. Inheritance of female sterility in barley. *Can. J. Plant Sci* **48**: 417–418.

Harwood WA, Bartlett JG, Alves SC, Perry M, Smedley MA, Leyland N, Snape JW. **2009**. Barley transformation using Agrobacterium-mediated techniques. *Methods in Molecular Biology*.

Himi E, Yamashita Y, Haruyama N, Yanagisawa T, Maekawa M, Taketa S. **2012**. Ant28 gene for proanthocyanidin synthesis encoding the R2R3 MYB domain protein (Hvmyb10) highly affects grain dormancy in barley. *Euphytica* **188**: 141–151.

Houston K, McKim SM, Comadran J, Bonar N, Druka I, Uzrek N, Cirillo E, Guzy-Wrobelska J, Collins NC, Halpin C, *et al.* 2013. Variation in the interaction between alleles of HvAPETALA2 and

microRNA172 determines the density of grains on the barley inflorescence. *Proceedings of the National Academy of Sciences* **110**: 16675–16680.

Hughes N, Oliveira HR, Fradgley N, Corke FMK, Cockram J, Doonan JH, Nibau C. **2019**. µ <scp>CT</scp> trait analysis reveals morphometric differences between domesticated temperate small grain cereals and their wild relatives. *The Plant Journal* **99**: 98–111.

Irish V. **2017**. The ABC model of floral development. *Current Biology* **27**: R887–R890.

Jack T, Brockman LL, Meyerowitz EM. **1992**. The homeotic gene APETALA3 of Arabidopsis thaliana encodes a MADS box and is expressed in petals and stamens. *Cell* **68**: 683–697.

Javelle M, Marco CF, Timmermans M. **2011**. In situ hybridization for the precise localization of transcripts in plants. *Journal of Visualized Experiments*.

Jeon JS, Jang S, Lee S, Nam J, Kim C, Lee SH, Chung YY, Kim SR, Lee YH, Cho YG, *et al.* 2000. leafy hull sterile1 is a homeotic mutation in a rice MADS box gene affecting rice flower development. *The Plant cell* **12**: 871–84.

Ji H, Han C-D, Lee G-S, Jung K-H, Kang D-Y, Oh J, Oh H, Cheon K-S, Kim SL, Choi I, *et al.* 2019. Mutations in the microRNA172 binding site of SUPERNUMERARY BRACT (SNB) suppress internode elongation in rice. *Rice (New York, N.Y.)* **12**: 62.

Jiang L, Ma X, Zhao S, Tang Y, Liu F, Gu P, Fu Y, Zhu Z, Cai H, Sun C, *et al.* 2019. The APETALA2-Like Transcription Factor SUPERNUMERARY BRACT Controls Rice Seed Shattering and Seed Size. *The Plant Cell* **31**: 17–36.

Jofuku KD, den Boer BGW, Van Montagu M, Okamuro JK. **1994**. Control of Arabidopsis flower and seed development by the homeotic gene APETALA2. *Plant Cell* **6**: 1211–1225.

Jost M, Taketa S, Mascher M, Himmelbach A, Yuo T, Shahinnia F, Rutten T, Druka A, Schmutzer T, Steuernagel B, *et al.* 2016. A homolog of Blade-On-Petiole 1 and 2 (BOP1/2) controls internode length and homeotic changes of the barley inflorescence. *Plant Physiology* **171**: pp.00124.2016.

Kellogg EA. **2015**. *Flowering Plants. Monocots*. Cham: Springer International Publishing AG.

Khanday I, Das S, Chongloi GL, Bansal M, Grossniklaus U, Vijayraghavan U. **2016**. Genome-Wide Targets Regulated by the OsMADS1 Transcription Factor Reveals Its DNA Recognition Properties. *Plant Physiology* **172**: 372–388.

Khanday I, Yadav SR, Vijayraghavan U. **2013**. Rice LHS1/OsMADS1 Controls Floret Meristem Specification by Coordinated Regulation of Transcription Factors and Hormone Signaling Pathways. *Plant Physiology* **161**: 1970–1983.

Kunst L, Klenz JE, Martinez-Zapater J, Haughn GW. **1989**. AP2 Gene Determines the Identity of Perianth Organs in Flowers of Arabidopsis thaliana. *The Plant Cell* **1**: 1195–1208.

Kyozuka J, Shimamoto K. **2002**. Ectopic expression of OsMADS3, a rice ortholog of AGAMOUS, caused a homeotic transformation of lodicules to stamens in transgenic rice plants. *Plant and Cell Physiology* **43**: 130–135.

Lee D-Y, An G. **2012**. Two AP2 family genes, SUPERNUMERARY BRACT (SNB) and OsINDETERMINATE SPIKELET 1 (OsIDS1), synergistically control inflorescence architecture and floral meristem establishment in rice. *The Plant Journal* **69**: 445–461.

Lee DY, Lee J, Moon S, Park SY, An G. **2007**. The rice heterochronic gene SUPERNUMERARY BRACT regulates the transition from spikelet meristem to floral meristem. *Plant Journal* **49**: 64–78.

Li N, Li Y. **2016**. Signaling pathways of seed size control in plants. *Current Opinion in Plant Biology* **33**: 23–32.

Li N, Xu R, Li Y. **2019**. Molecular Networks of Seed Size Control in Plants. *Annual Review of Plant Biology* **70**: 435–463.

Lombardo F, Yoshida H. **2015**. Interpreting lemma and palea homologies: a point of view from rice floral mutants . *Frontiers in Plant Science* **6**: 61.

Lu J, Magnani E. **2018**. Seed tissue and nutrient partitioning, a case for the nucellus. *Plant Reproduction* **31**: 309–317.

Lyu J, Wang D, Duan P, Liu Y, Huang K, Zeng D, Zhang L, Dong G, Li Y, Xu R, *et al.* 2020. Control of Grain Size and Weight by the GSK2-LARGE1/OML4 Pathway in Rice. *The Plant Cell* **32**: 1905–1918.

Ma X, Feng F, Zhang Y, Elesawi IE, Xu K, Li T, Mei H, Liu H, Gao N, Chen C, *et al.* 2019. A novel rice grain size gene OsSNB was identified by genome-wide association study in natural population (Z Zhang, Ed.). *PLOS Genetics* **15**: e1008191.

Ma X, Zhang Q, Zhu Q, Liu W, Chen Y, Qiu R, Wang B, Yang Z, Li H, Lin Y, *et al.* 2015. A Robust CRISPR/Cas9 System for Convenient, High-Efficiency Multiplex Genome Editing in Monocot and Dicot Plants. *Molecular Plant* **8**: 1274–1284.

Malcomber ST, Kellogg EA. **2004**. Heterogenous expression patterns and separate roles of the SEPALLATA gene LEAFY HULL STERILE1 in grasses. *Plant Cell* **16**: 1692–1706.

Malcomber ST, Preston JC, Reinheimer R, Kossuth J, Kellogg EA. **2006**. Developmental Gene Evolution and the Origin of Grass Inflorescence Diversity. In: Advances in Botanical Research. Academic Press, 425–481.

Mascher M, Gundlach H, Himmelbach A, Beier S, Twardziok SO, Wicker T, Radchuk V, Dockter C, Hedley PE, Russell J, *et al.* 2017. A chromosome conformation capture ordered sequence of the barley genome. *Nature* **544**: 427–433.

Modrusan Z, Reiser L, Feldmann KA, Fischer RL, Haughn GW. **1994**. Homeotic Transformation of Ovules into Carpel-like Structures in Arabidopsis. *The Plant Cell* **6**: 333–349.

Nair SK, Wang N, Turuspekov Y, Pourkheirandish M, Sinsuwongwat S, Chen G, Sameri M, Tagiri A, Honda I, Watanabe Y, *et al.* 2010. Cleistogamous flowering in barley arises from the suppression of microRNA-guided HvAP2 mRNA cleavage. *Proceedings of the National Academy of Sciences* **107**: 490–495.

Nayar S, Sharma R, Tyagi AK, Kapoor S. **2013**. Functional delineation of rice MADS29 reveals its role in embryo and endosperm development by affecting hormone homeostasis. *Journal of Experimental Botany* **64**: 4239–4253.

Nesi N, Debeaujon I, Jond C, Stewart AJ, Jenkins GI, Caboche M, Lepiniec L. **2002**. The TRANSPARENT TESTA16 Locus Encodes the ARABIDOPSIS BSISTER MADS Domain Protein and Is Required for Proper Development and Pigmentation of the Seed Coat. *The Plant Cell* **14**: 2463–2479.

Ohmori S, Kimizu M, Sugita M, Miyao A, Hirochika H, Uchida E, Nagato Y, Yoshida H. **2009**. MOSAIC FLORAL ORGANS1, an AGL6-like MADS box gene, regulates floral organ identity and meristem fate in rice. *Plant Cell* **21**: 3008–3025.

Ohto M -a., Fischer RL, Goldberg RB, Nakamura K, Harada JJ. **2005**. Control of seed mass by APETALA2. *Proceedings of the National Academy of Sciences* **102**: 3123–3128.

Ohto M, Floyd SK, Fischer RL, Goldberg RB, Harada JJ. **2009**. Effects of APETALA2 on embryo,

endosperm, and seed coat development determine seed size in Arabidopsis. *Sexual Plant Reproduction* **22**: 277–289.

Patil V, McDermott HI, McAllister T, Cummins M, Silva JC, Mollison E, Meikle R, Morris J, Hedley PE, Waugh R, *et al.* 2019. APETALA2 control of barley internode elongation. *Development* **146**: dev170373.

Paul MJ, Watson A, Griffiths CA. 2020. Linking fundamental science to crop improvement through understanding source and sink traits and their integration for yield enhancement (T Lawson, Ed.). *Journal of Experimental Botany* **71**: 2270–2280.

Pfaffl MW. 2001. A new mathematical model for relative quantification in real-time RT–PCR. *Nucleic Acids Research* **29**: e45–e45.

Prasad K, P. S, Kumar S, Kushalappa K, Vijayraghavan U. 2001. Ectopic expression of rice OsMADS1 reveals a role in specifying the lemma and palea, grass floral organs analogous to sepals. *Development Genes and Evolution* **211**: 281–290.

Prasad K, Parameswaran S, Vijayraghavan U. 2005. OsMADS1, a rice MADS-box factor, controls differentiation of specific cell types in the lemma and palea and is an early-acting regulator of inner floral organs. *The Plant Journal* **43**: 915–928.

Prasad K, Zhang X, Tobón E, Ambrose BA. 2010. The Arabidopsis B-sister MADS-box protein, GORDITA, represses fruit growth and contributes to integument development. *The Plant Journal* **62**: 203–214.

Radchuk V, Borisjuk L, Radchuk R, Steinbiss H-H, Rolletschek H, Broeders S, Wobus U. 2006. Jekyll Encodes a Novel Protein Involved in the Sexual Reproduction of Barley. *The Plant Cell* **18**: 1652–1666.

Radchuk V, Weier D, Radchuk R, Weschke W, Weber H. 2011. Development of maternal seed tissue in barley is mediated by regulated cell expansion and cell disintegration and coordinated with endosperm growth. *Journal of Experimental Botany*.

Ren D, Hu J, Xu Q, Cui Y, Zhang Y, Zhou T, Rao Y, Xue D, Zeng D, Zhang G, *et al.* 2018. FZP determines grain size and sterile lemma fate in rice. *Journal of Experimental Botany* **69**: 4853–4866.

Ren D, Li Y, He G, Qian Q. 2020. Multifloret spikelet improves rice yield. *New Phytologist* **225**: 2301–2306.

Ren D, Rao Y, Leng Y, Li Z, Xu Q, Wu L, Qiu Z, Xue D, Zeng D, Hu J, *et al.* 2016. Regulatory Role of OsMADS34 in the Determination of Glumes Fate, Grain Yield, and Quality in Rice. *Frontiers in Plant Science* **7**: 1853.

Ripoll JJ, Roeder AHK, Ditta GS, Yanofsky MF. 2011. A novel role for the floral homeotic gene APETALA2 during Arabidopsis fruit development. *Development* **138**: 5167 LP – 5176.

Ruan B, Shang L, Zhang B, Hu J, Wang Y, Lin H, Zhang A, Liu C, Peng Y, Zhu L, *et al.* 2020. Natural variation in the promoter of TGW2 determines grain width and weight in rice. *New Phytologist* **227**: 629–640.

Sakuma S, Schnurbusch T. 2020. Of floral fortune: tinkering with the grain yield potential of cereal crops. *New Phytologist* **225**: 1873–1882.

Schrager-Lavelle A, Klein H, Fisher A, Bartlett M. 2017. Grass flowers: An untapped resource for floral evo-devo. *Journal of Systematics and Evolution* **55**: 525–541.

Schubert R, Dobritzsch S, Gruber C, Hause G, Athmer B, Schreiber T, Marillonnet S, Okabe Y, Ezura H, Acosta IF, *et al.* 2019. Tomato myb21 acts in ovules to mediate jasmonate-regulated fertility. *Plant Cell*.

Si L, Chen J, Huang X, Gong H, Luo J, Hou Q, Zhou T, Lu T, Zhu J, Shangguan Y, *et al.* 2016. OsSPL13 controls grain size in cultivated rice. *Nature Genetics* **48**: 447–456.

Simons KJ, Fellers JP, Trick HN, Zhang Z, Tai Y-S, Gill BS, Faris JD. **2006**. Molecular characterization of the major wheat domestication gene Q. *Genetics* **172**: 547–55.

Song X-J, Huang W, Shi M, Zhu M-Z, Lin H-X. **2007**. A QTL for rice grain width and weight encodes a previously unknown RING-type E3 ubiquitin ligase. *Nature Genetics* **39**: 623–630.

Song G, Sun G, Kong X, Jia M, Wang K, Ye X, Zhou Y, Geng S, Mao L, Li A. **2019**. The soft glumes of common wheat are sterile-lemmas as determined by the domestication gene Q. *The Crop Journal* **7**: 113–117.

Sormacheva I, Golovnina K, Vavilova V, Kosuge K, Watanabe N, Blinov A, Goncharov NP. **2015**. Q gene variability in wheat species with different spike morphology. *Genetic Resources and Crop Evolution* **62**: 837–852.

Sreenivasulu N, Radchuk V, Strickert M, Miersch O, Weschke W, Wobus U. **2006**. Gene expression patterns reveal tissue-specific signaling networks controlling programmed cell death and ABA-regulated maturation in developing barley seeds. *Plant Journal*.

Theißen G, Melzer R, Rümpler F. **2016**. MADS-domain transcription factors and the floral quartet model of flower development: linking plant development and evolution. *Development* **143**: 3259 LP – 3271.

Thiel J, Weier D, Sreenivasulu N, Strickert M, Weichert N, Melzer M, Czauderna T, Wobus U, Weber H, Weschke W. **2008**. Different Hormonal Regulation of Cellular Differentiation and Function in Nucellar Projection and Endosperm Transfer Cells: A Microdissection-Based Transcriptome Study of Young Barley Grains. *Plant Physiology* **148**: 1436–1452.

Tsuchiya T. **1962**. *Annual report on breeding of malting barley*.

Waddington SR, Cartwright PM, Wall PC. **1983**. A Quantitative Scale of Spike Initial and Pistil Development in Barley and Wheat. *Annals of Botany* **51**: 119–130.

Wang S, Wu K, Yuan Q, Liu X, Liu Z, Lin X, Zeng R, Zhu H, Dong G, Qian Q, *et al.* 2012. Control of grain size, shape and quality by OsSPL16 in rice. *Nature Genetics* **44**: 950–954.

Wilkinson LG, Bird DC, Tucker MR. **2018**. Exploring the Role of the Ovule in Cereal Grain Development and Reproductive Stress Tolerance. *Annual Plant Reviews online*: 181–216.

Wilkinson LG, Yang X, Burton RA, Würschum T, Tucker MR. **2019**. Natural Variation in Ovule Morphology Is Influenced by Multiple Tissues and Impacts Downstream Grain Development in Barley (Hordeum vulgare L.). *Frontiers in plant science* **10**: 1374.

Xie Q, Li N, Yang Y, Lv Y, Yao H, Wei R, Sparkes DL, Ma Z. **2018**. Pleiotropic effects of the wheat domestication gene Q on yield and grain morphology. *Planta* **247**: 1089–1098.

Xie Q, Mayes S, Sparkes DL. **2015**. Carpel size, grain filling, and morphology determine individual grain weight in wheat. *Journal of Experimental Botany* **66**: 6715–6730.

Xu W, Fiume E, Coen O, Pechoux C, Lepiniec L, Magnani E. **2016**. Endosperm and Nucellus Develop Antagonistically in Arabidopsis Seeds. *The Plant Cell* **28**: 1343 LP – 1360.

Yamaguchi T, Lee DY, Miyao A, Hirochika H, An G, Hirano HY. **2006**. Functional diversification of the two C-class MADS box genes OSMADS3 and OSMADS58 in Oryza sativa. *Plant Cell*.

Yang X, Wu F, Lin X, Du X, Chong K, Gramzow L, Schilling S, Becker A, Theißen G, Meng Z. **2012**. Live and Let Die - The Bsister MADS-Box Gene OsMADS29 Controls the Degeneration of Cells in Maternal Tissues during Seed Development of Rice (Oryza sativa) (JL Heazlewood, Ed.). *PLoS ONE* **7**: e51435.

Yant L, Mathieu J, Dinh TT, Ott F, Lanz C, Wollmann H, Chen X, Schmid M. **2010**. Orchestration of the Floral Transition and Floral Development in Arabidopsis by the Bifunctional Transcription Factor APETALA2. *The Plant Cell* **22**: 2156–2170.

Yin L-L, Xue H-W. **2012**. The MADS29 Transcription Factor Regulates the Degradation of the Nucellus and the Nucellar Projection during Rice Seed Development. *The Plant Cell* **24**: 1049–1065.

Yoshida H. **2012**. Is the lodicule a petal: Molecular evidence? *Plant Science* **184**: 121–128.

You X, Zhu S, Zhang W, Zhang J, Wang C, Jing R, Chen W, Wu H, Cai Y, Feng Z, *et al.* 2019. Os PEX5 regulates rice spikelet development through modulating jasmonic acid biosynthesis. *New Phytologist* **224**: 712–724.

Zhang X, Wang J, Huang J, Lan H, Wang C, Yin C, Wu Y, Tang H, Qian Q, Li J, *et al.* 2012. Rare allele of OsPPKL1 associated with grain length causes extra-large grain and a significant yield increase in rice. *Proceedings of the National Academy of Sciences* **109**: 21534–21539.

Zhao L, Kim Y, Dinh TT, Chen X. **2007**. miR172 regulates stem cell fate and defines the inner boundary of APETALA3 and PISTILLATA expression domain in Arabidopsis floral meristems. *The Plant Journal* **51**: 840–849.

Zhao D-S, Li Q-F, Zhang C-Q, Zhang C, Yang Q-Q, Pan L-X, Ren X-Y, Lu J, Gu M-H, Liu Q-Q. **2018**. GS9 acts as a transcriptional activator to regulate rice grain shape and appearance quality. *Nature Communications* **9**: 1240.

FIGURE LEGENDS

Fig. 1. *gigas1.a* mutants show altered reproductive organ and grain morphology. Bowman and *gigas1.a*: (A) spikes; (B) spike density (nodes/ cm); (C) spikelets (white arrows show distal end of the lemma and red arrows denote the awn-lemma boundary); (D) lemma length (mm); (E) Length of awn length (cm) on lemmas (left) and glumes (right); (F) lemmas; (G) glumes; (H) lodicules. (I) Scanning electron micrographs (SEMs) of Bowman and *gigas1.a* lodicules. (J) SEM showing ectopic hairs on *gigas1.a* lodicules (arrow). (K) SEMs of Bowman and *gigas1.a* stigmas. Arrow points to stigma hairs on Bowman. Right panel shows a magnification of a single *gigas1.a* stigma lacking hairs. (L-M) Bowman and *gigas1.a* (L) hull covered and (M) hull removed grains. (N) Violin plots of Bowman (n=97), *gigas1.a* (n=69) and *Zeo1.b* (n=72) grains show the probability distribution of grain length (mm). (O) *Zeo1.b* spikelets show glume to lemma conversion (white arrows indicate glume position

organ). Box plots (B,D,E) show 25th and 75th percentile, red line show the median, whiskers show 1.5* the interquartile range. Scale bars: 2cm (A,F); 2mm (C,G,L,M); 500µm (I,J,K (left, centre)); 100µm (K right); 1mm (N)). *** p<0.001 (*t*-test, two-tailed). (B,D,E) n=8/ genotype.

Fig. 2. Mapping of *gigas1.a* and gene editing of *HvAPETALA2*. (A) Grey block on chromosome 2H indicates introgression from Golden Melon in *gigas1.a* BW381. JHI-50k-2016 SNP markers and genes shown along with their physical position (Mbp). Missing markers (red) delineate a 1.3Mbp deletion overlapping seven high confidence gene models, including *HORVU2Hr1G113880* (*HvAP2*) and *HORVU2Hr1G113940*; (B) RT-qPCR of *HvAPETALA2* (*HvAP2*) transcripts in Bowman, *gigas1.a*, and *Zeo1.b* spikes. Individual points are independent biological replicates. (C) *HvAP2* gene model with sequences encoding the APETALA2 DNA binding domains (grey) and miR172 binding site (black). Nucleotides 167 to 239 and their corresponding protein sequences shown underneath for Golden Promise (GP), *hvap2-1*, and *hvap2-2*. Lines over GP sequence indicate guide RNA target (red) and protospacer adjacent motif (PAM, blue). Dashes indicate deleted bases and triangles indicate deletion length in *hvap2-1*, and *hvap2-2*. (D-H) Phenotypes of GP, *hvap2-1* and *hvap2-2*. (D) Spikelets. (E) Grains with hull on (left) and removed (right). (F) Lodicules. (G) Arrow shows transformation of lodicule to bract in *hvap2-2*. (H) Scanning electron micrograph showing ectopic hairs on *hvap2-2* lodicules. Scale bars: 2mm (D,E); 1mm (F); 100µm (H).

Fig. 3. *HvAPETALA2* regulates early spikelet organogenesis and gene expression. (A,B) Scanning electron micrographs (SEMs) of Bowman and *Zeo1.b* spikelets at (A) Waddington stage 4 (WD4) and (B) WD5.5. Arrows point to homeotic glume to lemma conversions in *Zeo1.b*. (C) SEMs of WD4, WD5.5 and WD7 Bowman, *gigas1.a*, and *Zeo1.b* with lemmas removed and inner floret primordia false coloured: lodicules, yellow; stamens, blue; carpel, red. (D) qRT-PCR of *HvMADS1* and *HvMADS58* mRNA in Bowman, *Zeo1.b* and *gigas1.a* spikelets. Individual points are independent

biological replicates. (E, F) In situ hybridisation of *HvMADS1* probe (E) WD4 and (F) WD7. Scale bars: 1mm (A); 0.5mm (B); 100µm (C); 1mm (E,F).

Fig. 4. *HvAPETALA2* alleles influence grain maturation and gene expression. (A-B) Bowman, *gigas1.a*, and *Zeo1.b* caryopses parameters measured at preanthesis (PA) and days post anthesis (DPA). (A) caryopsis length (mm). (B) caryopsis width (mm). (C-F) Grain ultrastructure in Bowman, *Zeo1.b* and *gigas1.a* at 5 DPA (C,E) and 10 DPA (D,F). (C) Arrows show provasculature strands. (D) Arrows show degradation of the nucellar projection. (G) *HvAP2* in situ hybridisation in pre-anthesis spikelets (top panel) and caryopses. (H) qRT-PCR of *HvMADS29*, *HvJIP23* and *HvJIP60* mRNA in Bowman and *gigas1.a* caryopses at 5 DPA. Individual points are independent biological replicates. ca, carpel; cc, cross cells; ch, chlorenchyma; ii, inner integument; ma, maternal aleurone; ms, mesocarp; np, nucellar projection; nu, nucellus epidermis; eil, extra integument layer; pem, pericarp mesocarp; ov, ovary; ps, pigment strand; vb, vascular bundle; se, starchy endosperm; t, testa; tc, tube cells. (A-B) n=5/ genotype. Box plots show the median (red line), 25th and 75th percentile, whiskers show 1.5* the interquartile range. *Significant difference between *gigas1.a* and Bowman; ^Significant difference between *Zeo1.b* and Bowman, $p<0.05$ (Dunn's post-hoc test).

Fig. 5. *HvMADS29* controls post-fertilisation development. (A) *HvMADS29* expression in ovary and caryopses based on RNA-seq. (B) *HvMADS29* in situ hybridisation on developing caryopses. Upper panel shows caryopsis section and lower panel shows higher magnification of the nucellar projection region. (C) *HvMADS29* gene model shows coding region sequence between nucleotides 55-195 and corresponding protein sequence for Golden Promise (GP) and *hvmads29-2*. Lines over GP sequence indicate guide RNA target (red) and protospacer adjacent motif (PAM, blue). Dash in *hvmads29* indicates the deleted base. (D) Mature GP and *hvmads29* caryopses. (E,F) GP and *hvmads29* caryopses at 0,5 and 10 days post anthesis (DPA). (E) Whole. (F) Sections show vascular bundles in

the nucellus projection. For each genotype, left lane, calcofluor white staining (cyan) and auto fluorescence (red), right lane, toluidine blue staining. Scale bars: 100µm (B upper panel); 50µm (B lower panel); 2mm (D,E); 50µm (F).

Fig. 6. Genetic analyses between *gigas1.a*, *lax.a* and *Zeo1.b*. (A,B) Spike, (C-H) spikelet, and (I,J) grain phenotypes in Bowman, *gigas1.a*, *Zeo1.b*, *lax.a*, *gigas1.a lax.a* and *Zeo1.b lax.a*. (A) Spikes. (B) Spike density (nodes/ cm). (C) Glume position organs. (D) Glume awn length (cm). (E) Palea/lemma position organs. (F) Lemma length (cm). (G) Lodicule and stamen position organs. (H) Lodicule and stamen organ counts per spikelet. (I) Grain. (J) Grain length (mm). Box plots show the median (red line), 25th and 75th percentile, whiskers show 1.5* the interquartile range and outliers as dots. Letters indicate significant difference ($p<0.05$; Tukey HSD). n= 8/ genotype. Scale bars: 2mm (A-G, apart from *Zeo1.b lax.a* in C, 2cm); 0.5 cm (I).

Fig 7. Model of HvAP2 function with putative up and downstream regulators. HvAP2 has multiple roles in pre- and post-fertilisation development. Diagrams underneath each role show the tissue involved. HvAP2 promotes the transition from spikelet to floret identity and perianth formation. miR172 regulation of HvAP2 is necessary to exclude floret/perianth identity from the glume primordia. These roles may be mediated by HvAP2 upregulation of *HvMADS1*. Elevated HvAP2 function represses stamen formation in the lodicule whorl, potentially by down-regulating of HvMADS3. HvAP2 promotes stigmatic branching, associated with *HvMADS58* expression. HvAP2 inhibits integument layer proliferation and promotes integument degradation. HvAP2 limits final grain length by restricting pericarp cell number and length. HvAP2 promotes nucellar tissue elimination, associated with *HvMADS29* expression, associated with endosperm growth and grain widening. HvBOP2 may promote HvAP2 function in the lodicule and grain through unknown

1002 mechanisms. Yellow colour in integument proliferation, grain length, nucellar elimination and grain

1003 width diagrams indicates integuments, pericarp, nucellar projection and endosperm, respectively.


A
Bw
gigas1.a

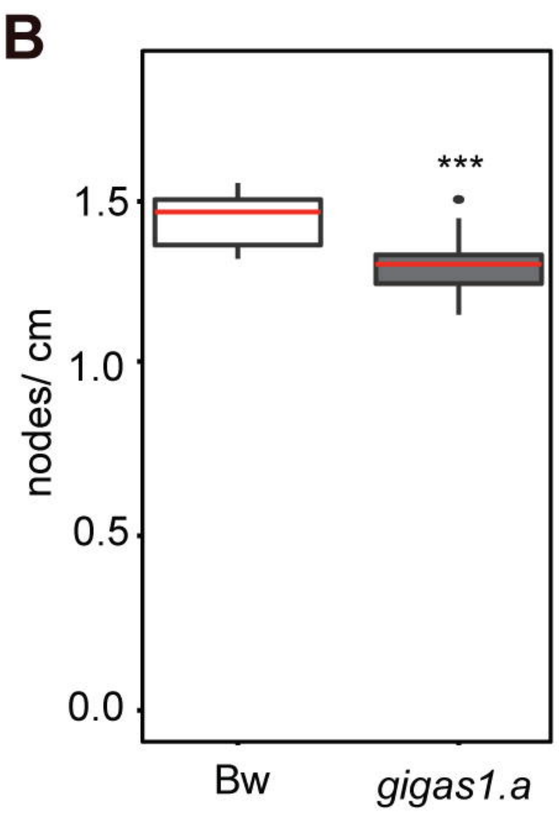
B
nodes/ cm
1.5
1.0
0.5
0.0
***
Bw
gigas1.a


C
Bw
gigas1.a

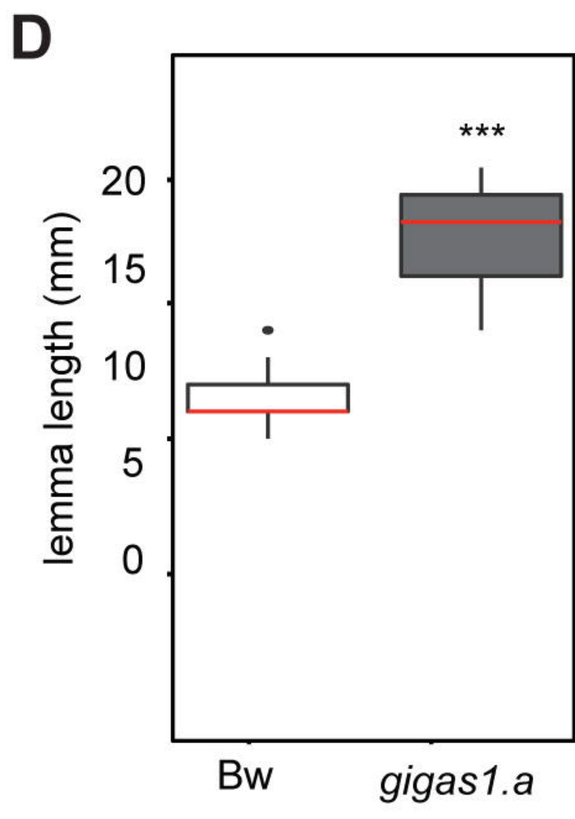
D
lemma length (mm)
20
15
10
5
0
***
Bw
gigas1.a

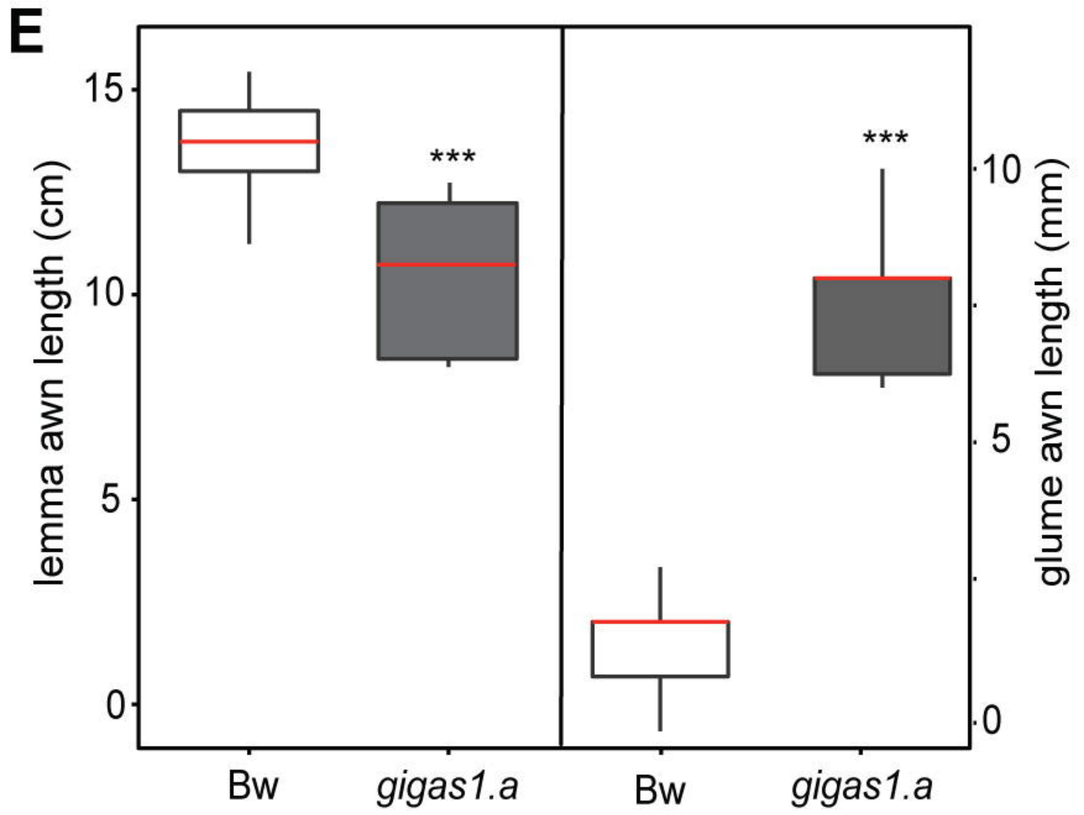
E
lemma awn length (cm)
15
10
5
0
***
glume awn length (mm)
10
5
0
***
Bw
gigas1.a
Bw
gigas1.a

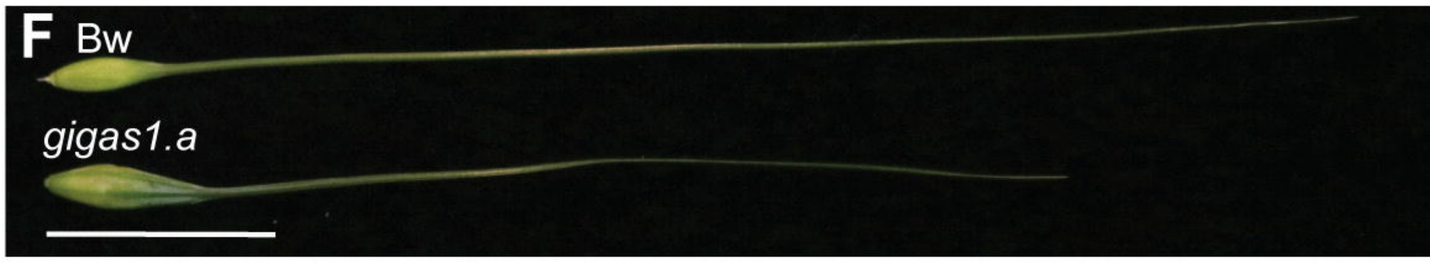
F
Bw
gigas1.a


G
Bw
gigas1.a


H
Bw
gigas1.a

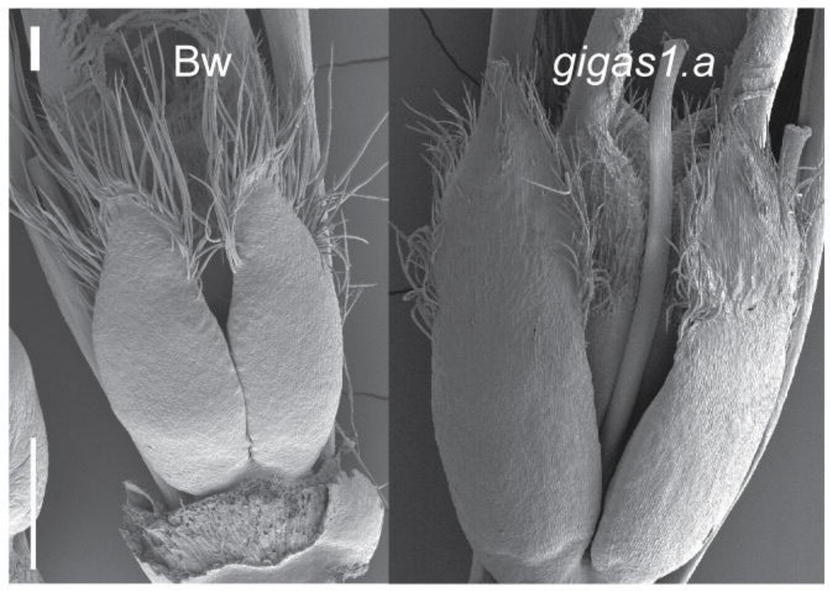
I
Bw
gigas1.a

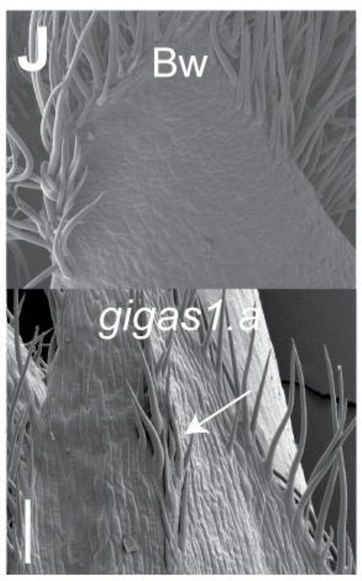
J
Bw
gigas1.a

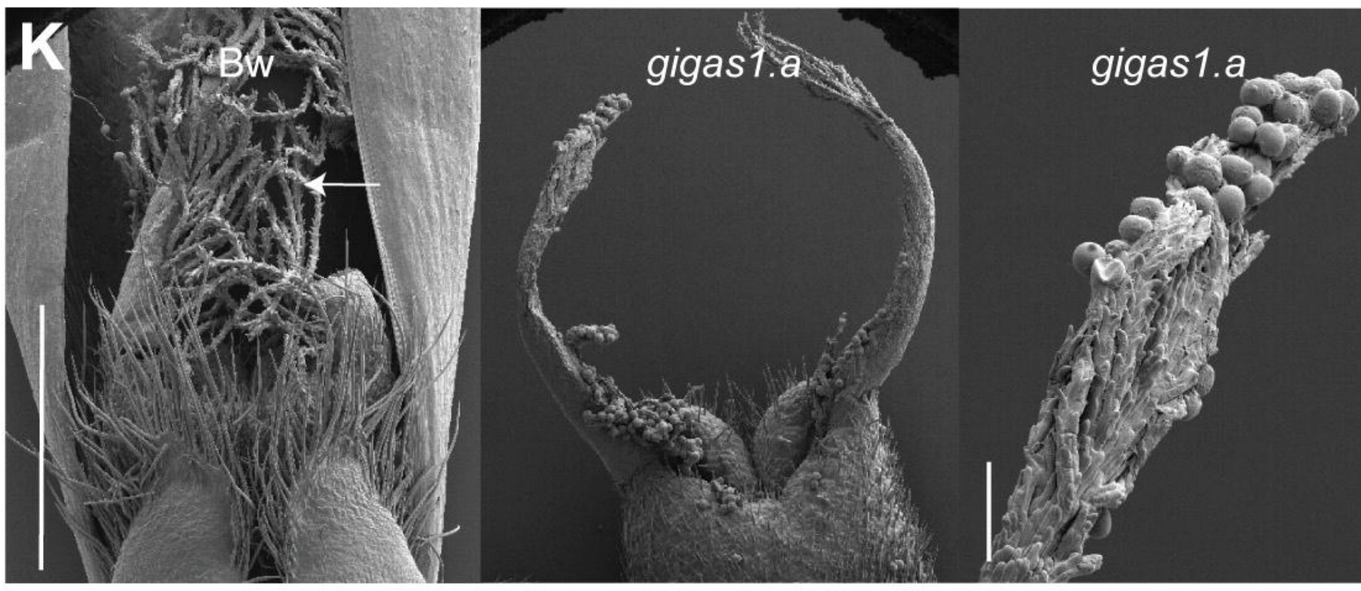
K
Bw
gigas1.a
gigas1.a


L
Bw
gigas1.a


M
Bw
gigas1.a

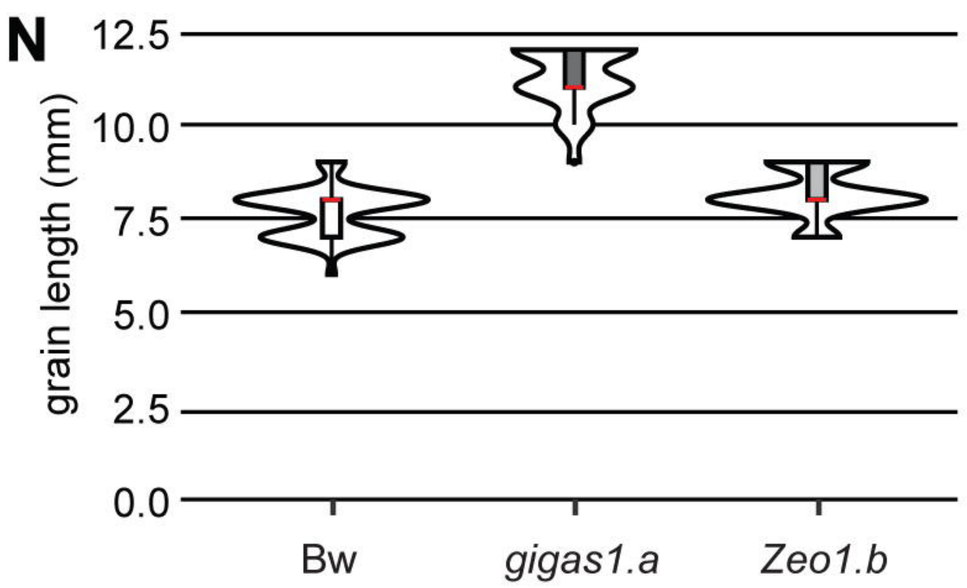
N
grain length (mm)
12.5
10.0
7.5
5.0
2.5
0.0
Bw
gigas1.a
Zeo1.b


O
Bw
Zeo1.b

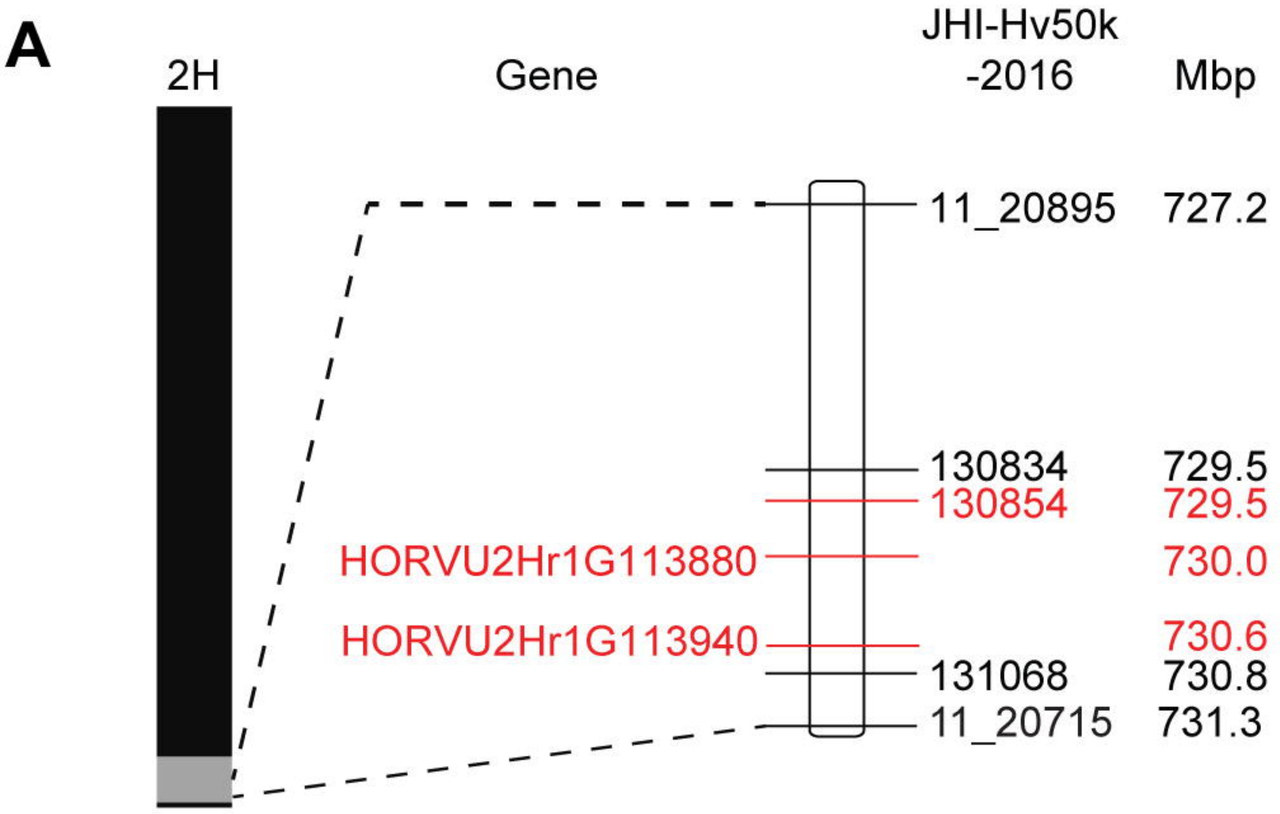
A
2H
Gene
JHI-Hv50k
-2016
Mbp
11_20895
727.2
130834
729.5
130854
729.5
HORVU2Hr1G113880
730.0
HORVU2Hr1G113940
730.6
131068
730.8
11_20715
731.3

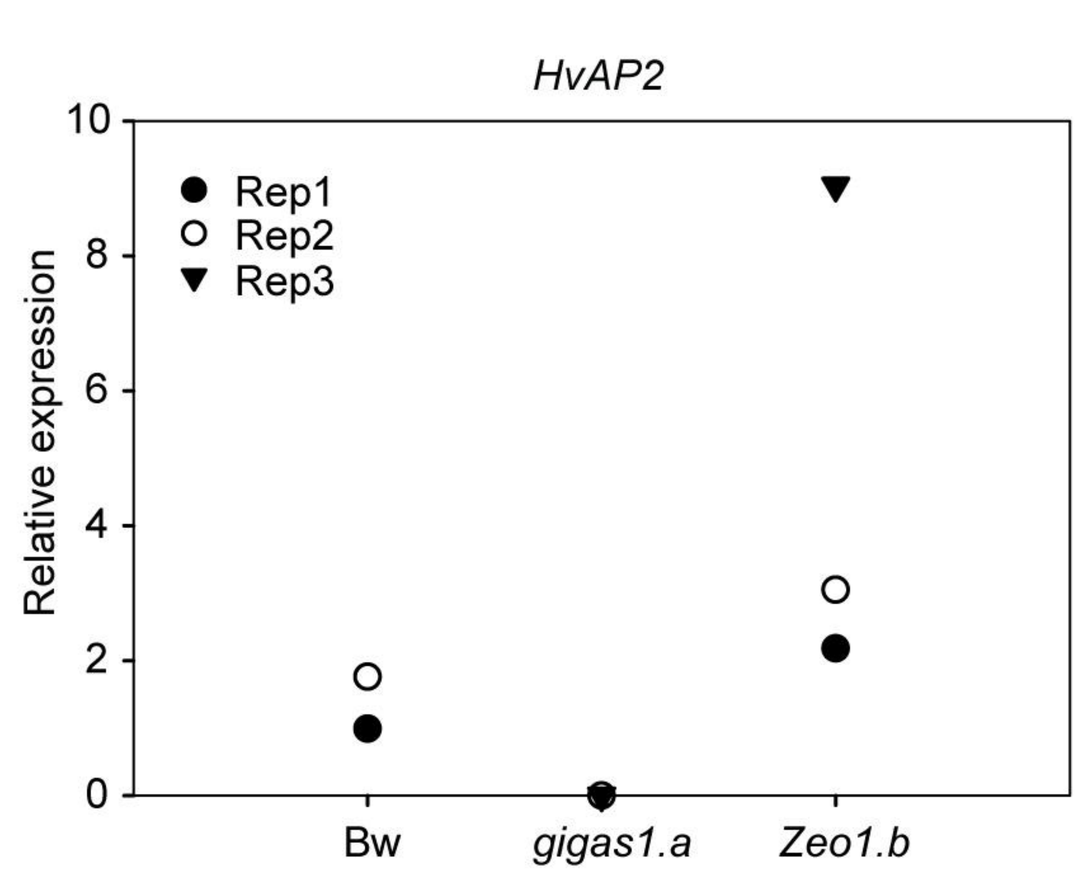
B
HvAP2
Relative expression
Rep1
Rep2
Rep3
Bw
gigas1.a
Zeo1.b

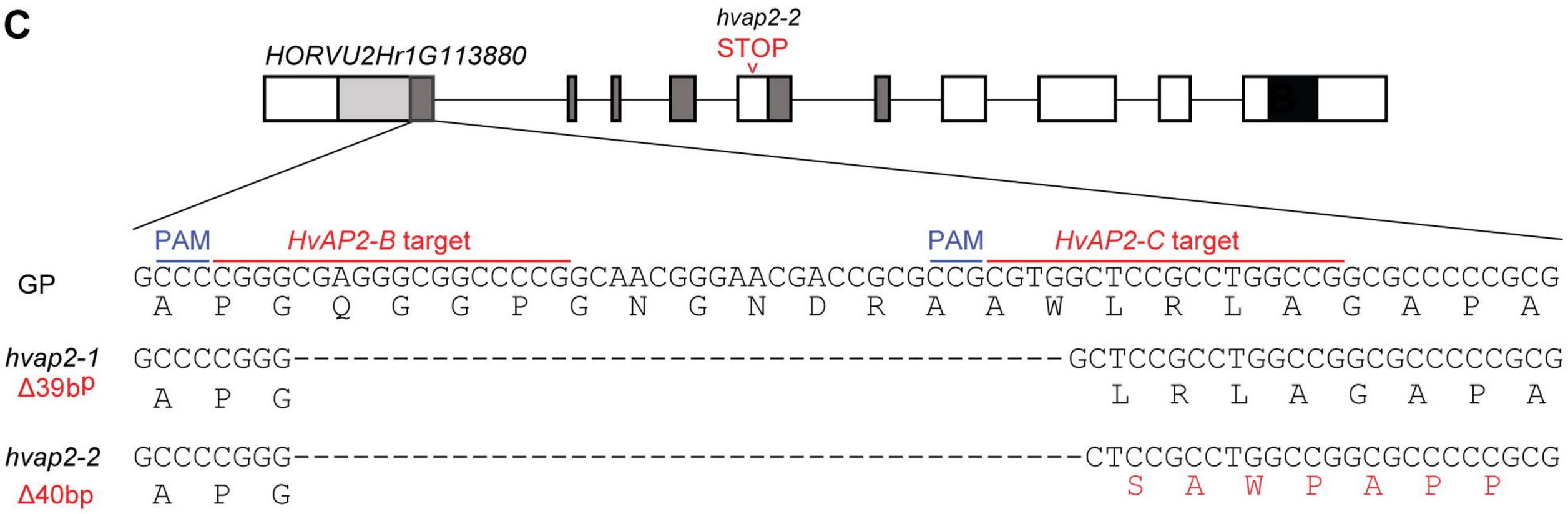
C
HORVU2Hr1G113880
hvap2-2
STOP
PAM
HvAP2-B target
PAM
HvAP2-C target
GP
GCCCCGGGCGAGGGCGGCCCCGGCAACGGGAACGACCGCGCCGCGTGGCTCCGCCTGGCCGGCGCCCCCGCG
A P G Q G G P G N G N D R A A W L R L A G A P A
hvap2-1
Δ39bp
GCCCCGGG----------GCTCCGCCTGGCCGGCGCCCCCGCG
A P G L R L A G A P A
hvap2-2
Δ40bp
GCCCCGGG----------CTCCGCCTGGCCGGCGCCCCCGCG
S A W P A P P

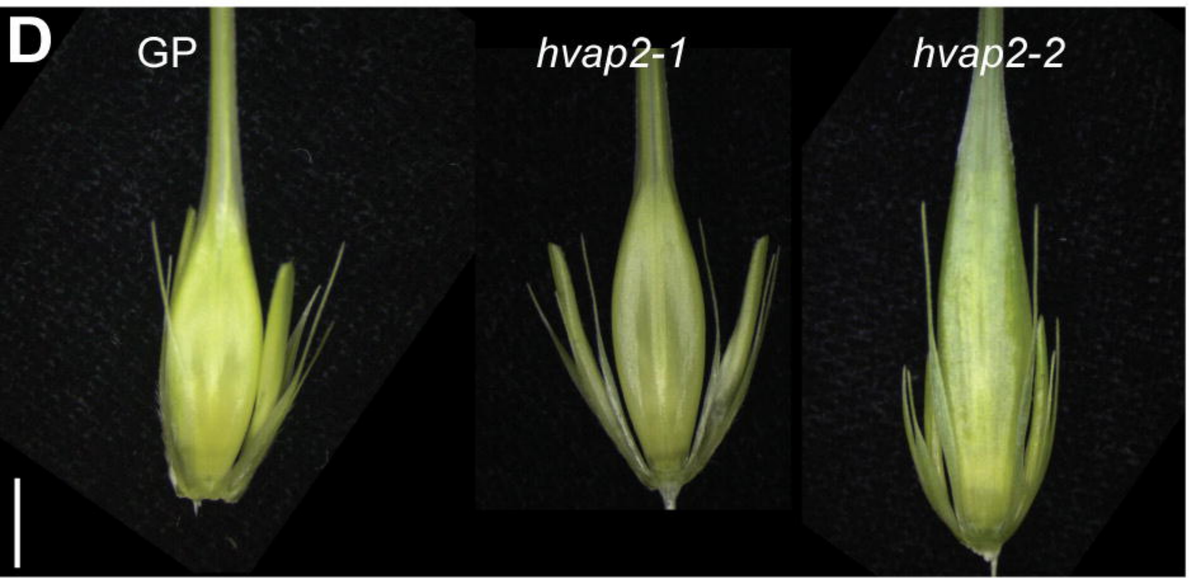
D
GP
hvap2-1
hvap2-2


E
GP
hvap2-1
hvap2-2

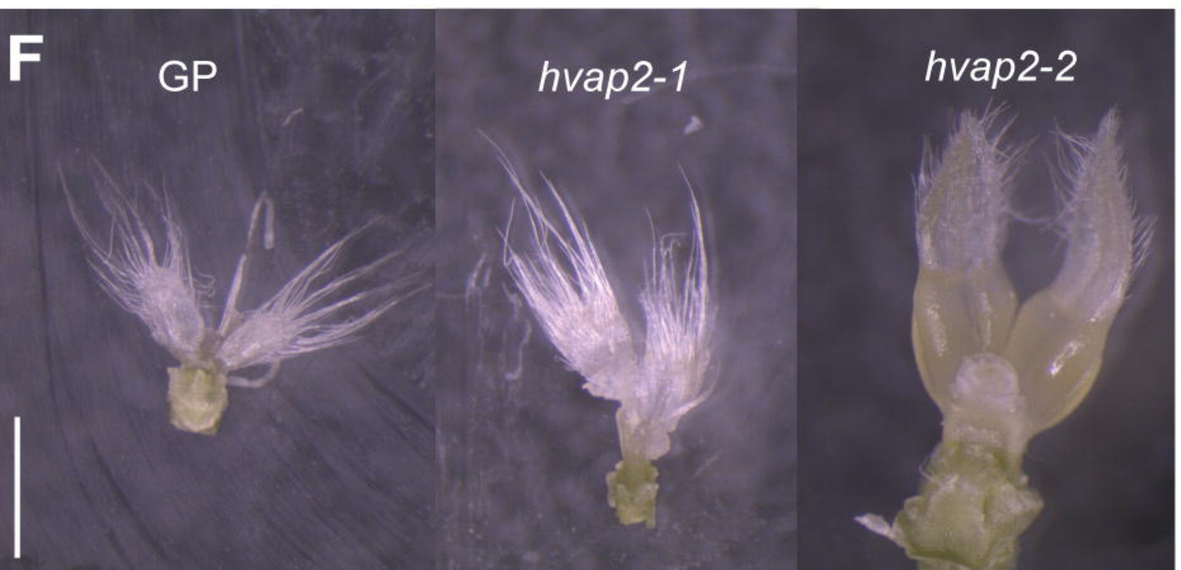
F
GP
hvap2-1
hvap2-2

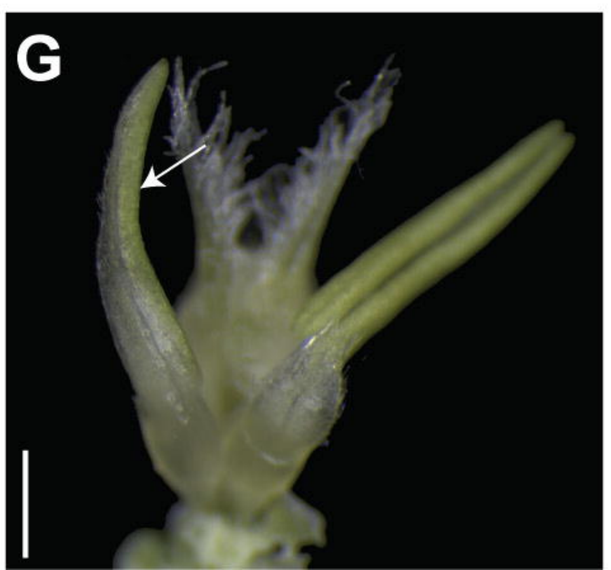
G

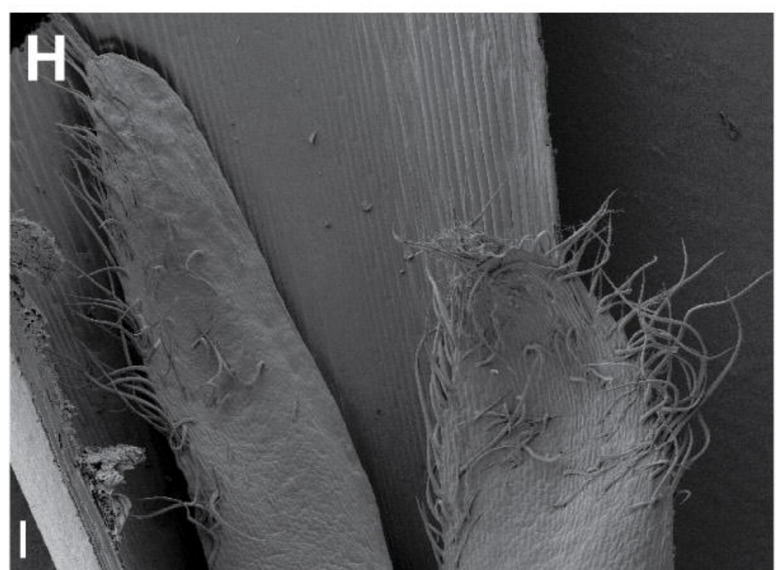
H

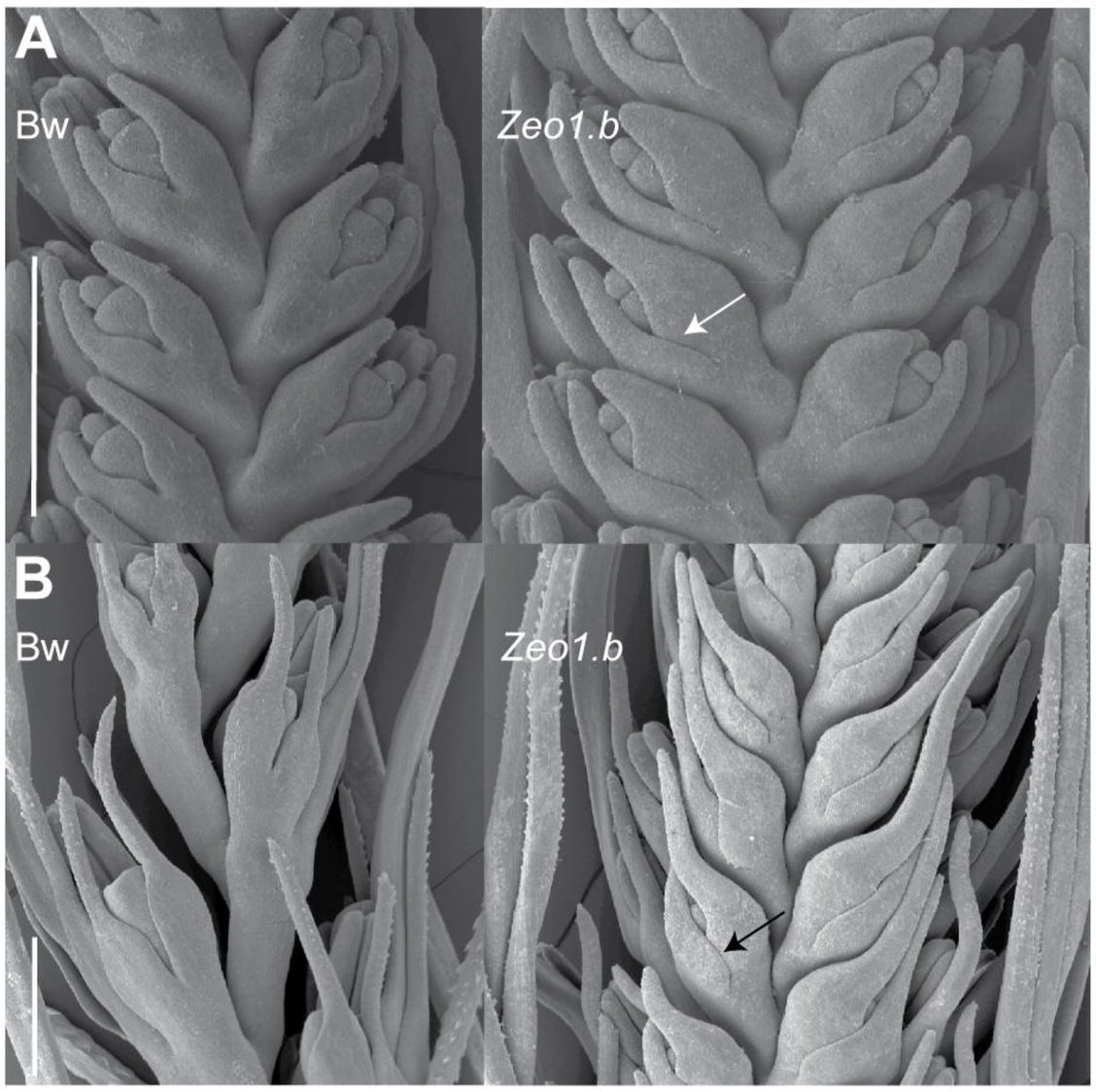
A
Bw
Zeo1.b
B
Bw
Zeo1.b

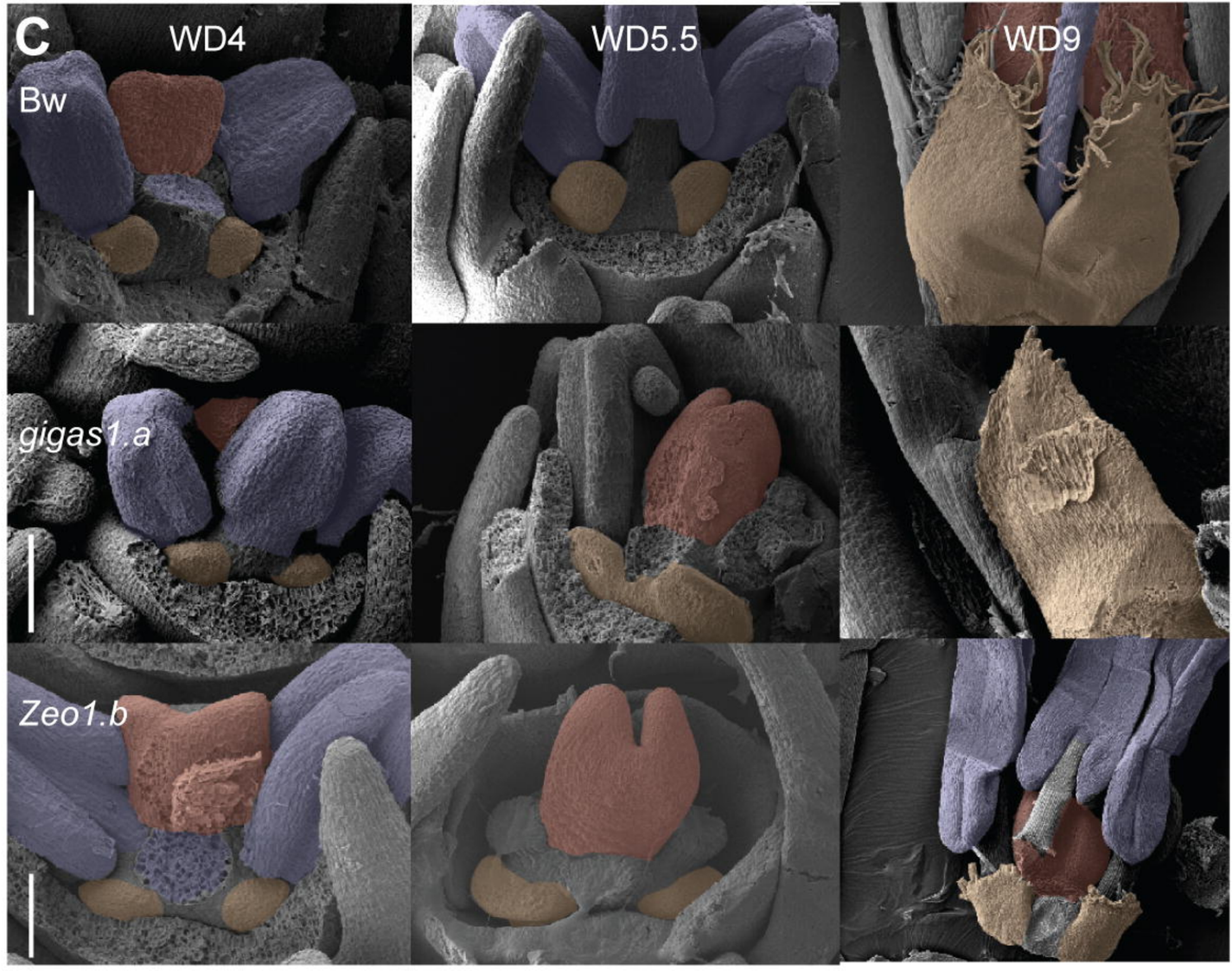
C
WD4
WD5.5
WD9
Bw
gigas1.a
Zeo1.b

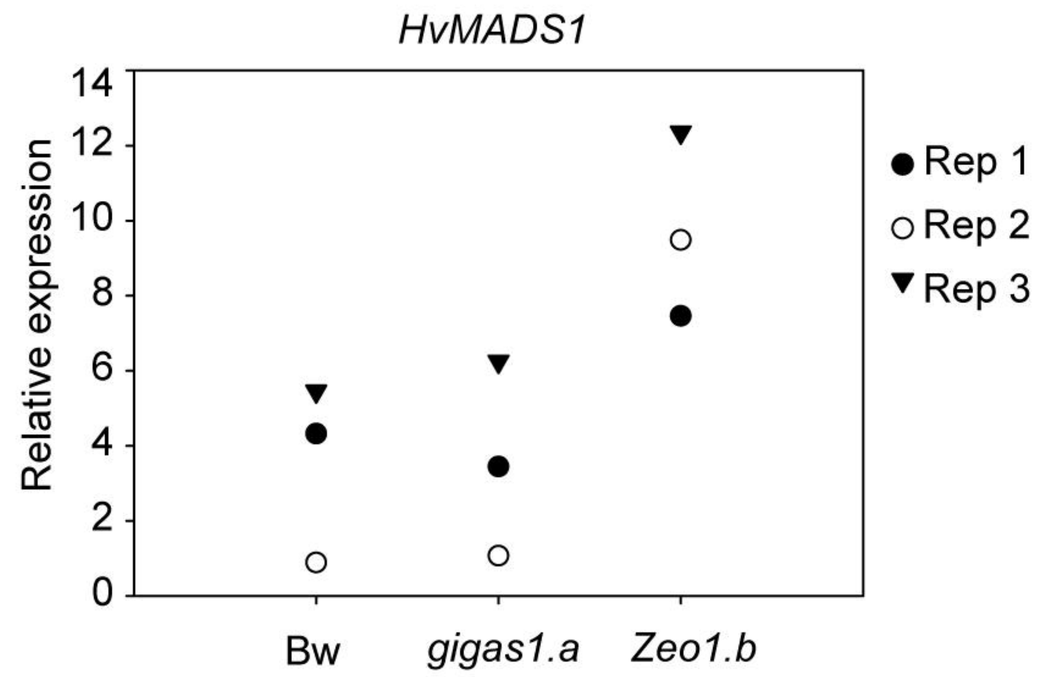
D
HvMADS1
Relative expression
14
12
10
8
6
4
2
0
Rep 1
Rep 2
Rep 3
Bw
gigas1.a
Zeo1.b

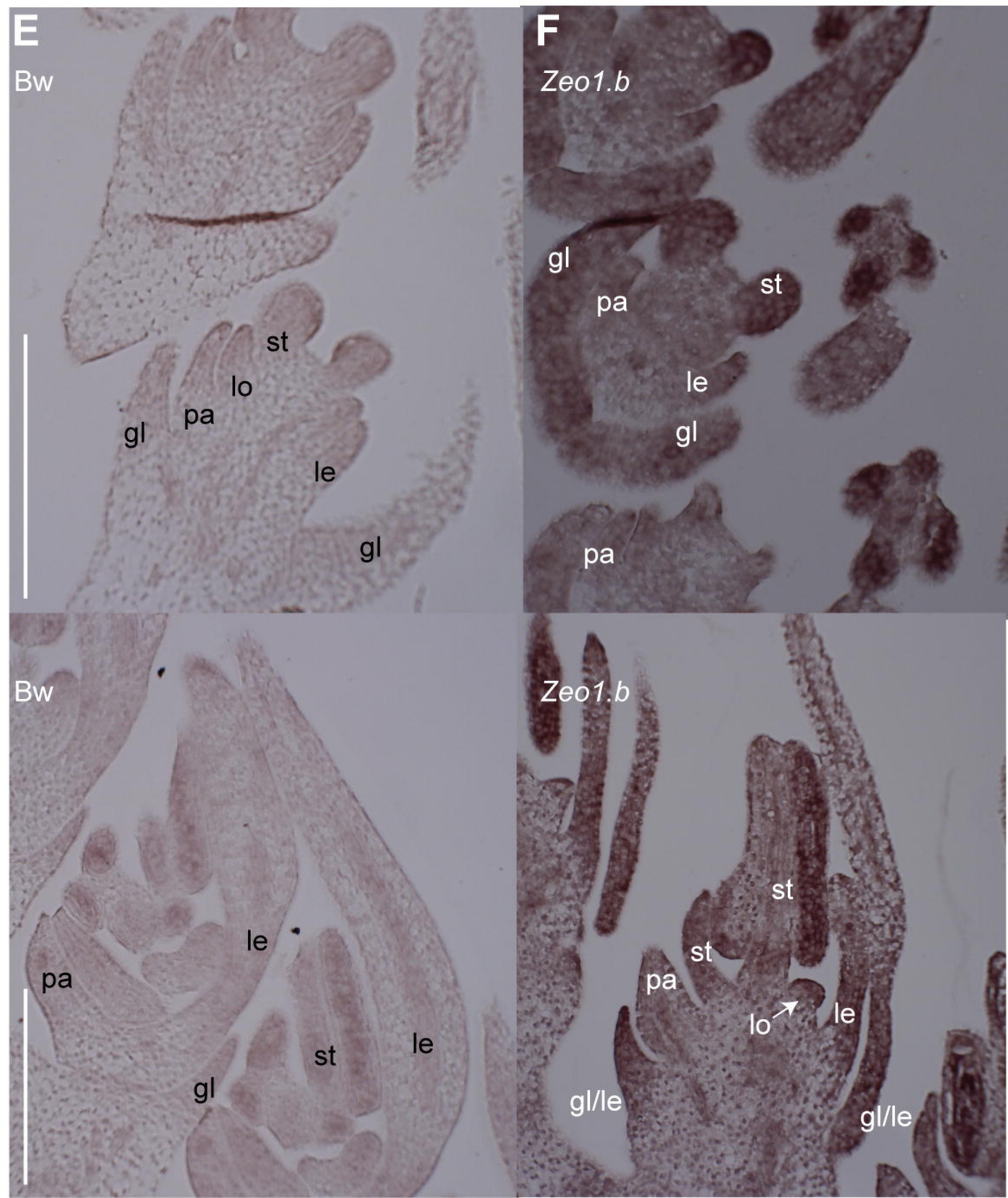
E
Bw
st
lo
pa
gl
le
gl
F
Zeo1.b
gl
pa
st
le
gl
pa
Bw
le
pa
st
le
gl
Zeo1.b
st
st
pa
lo
le
gl/le
gl/le

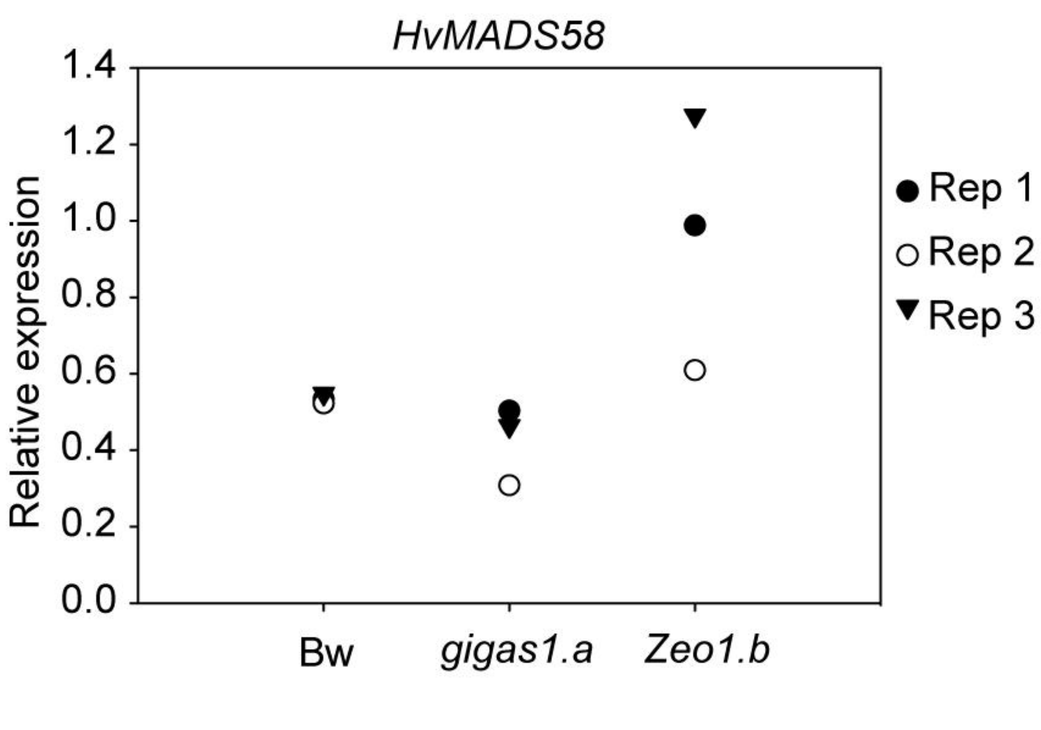
HvMADS58
Relative expression
1.4
1.2
1.0
0.8
0.6
0.4
0.2
0.0
Rep 1
Rep 2
Rep 3
Bw
gigas1.a
Zeo1.b

A

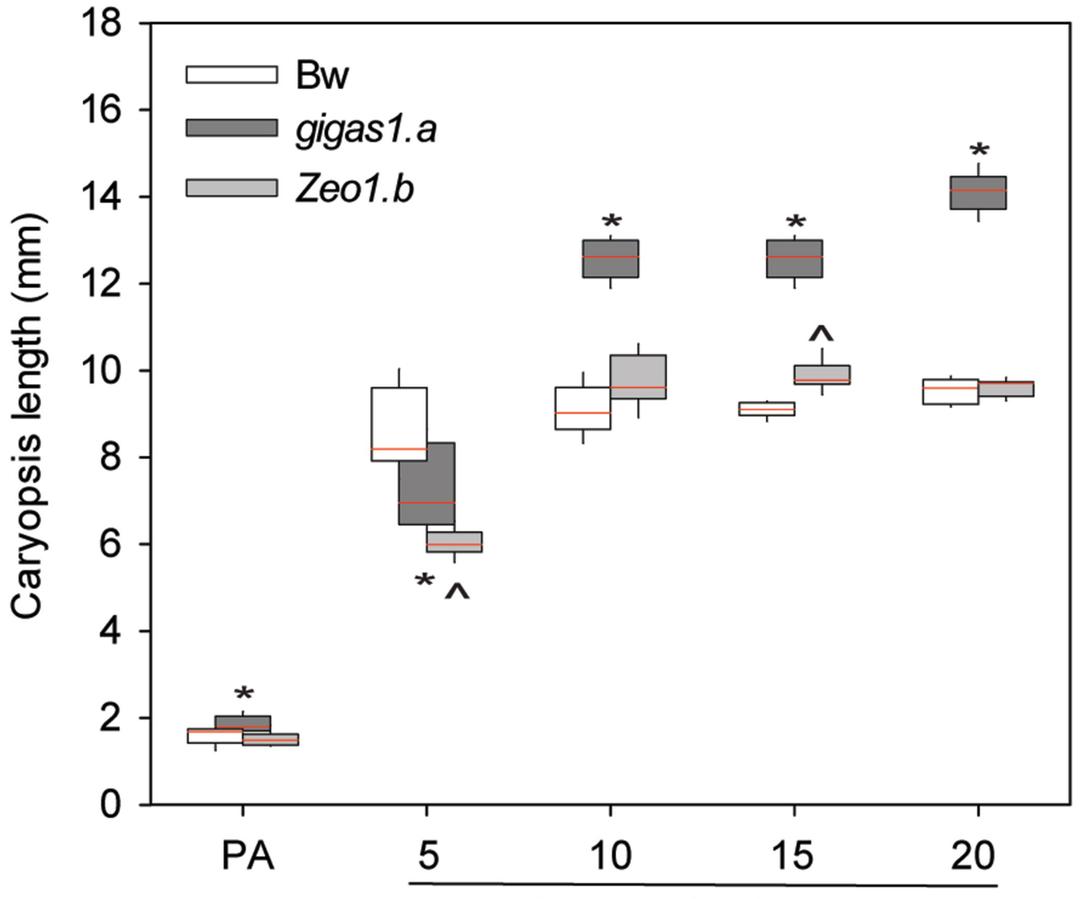

B

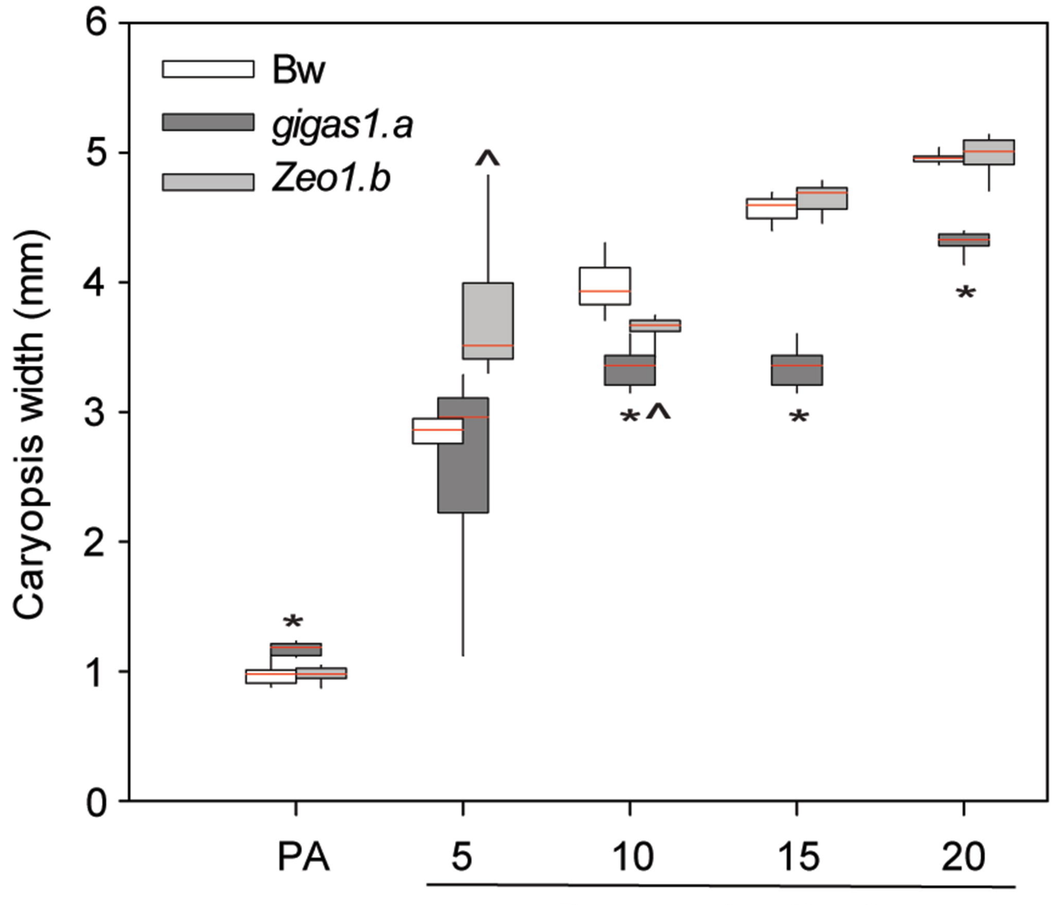

C

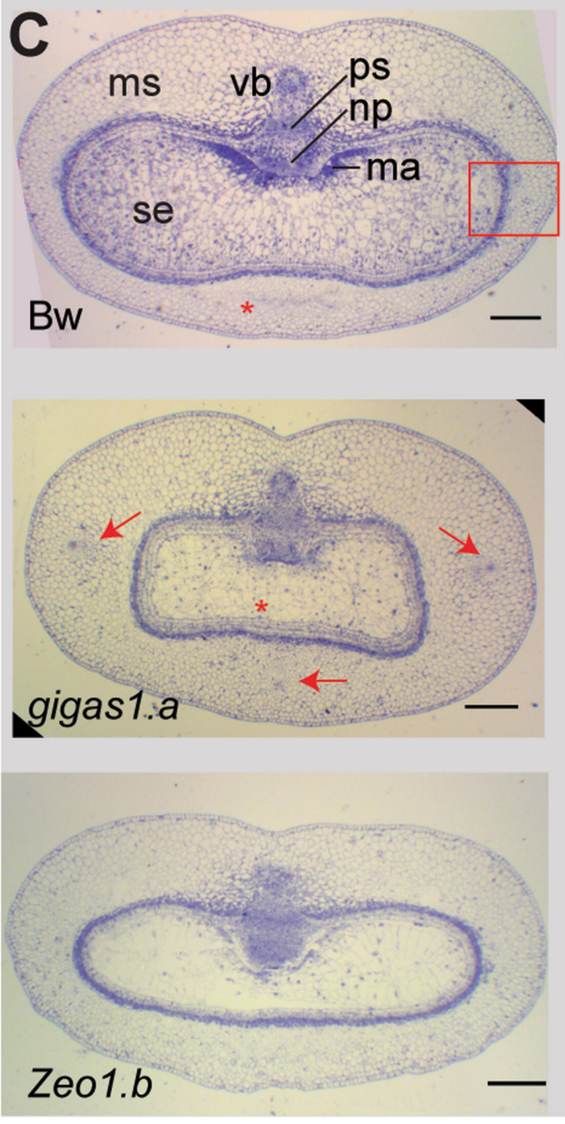

D

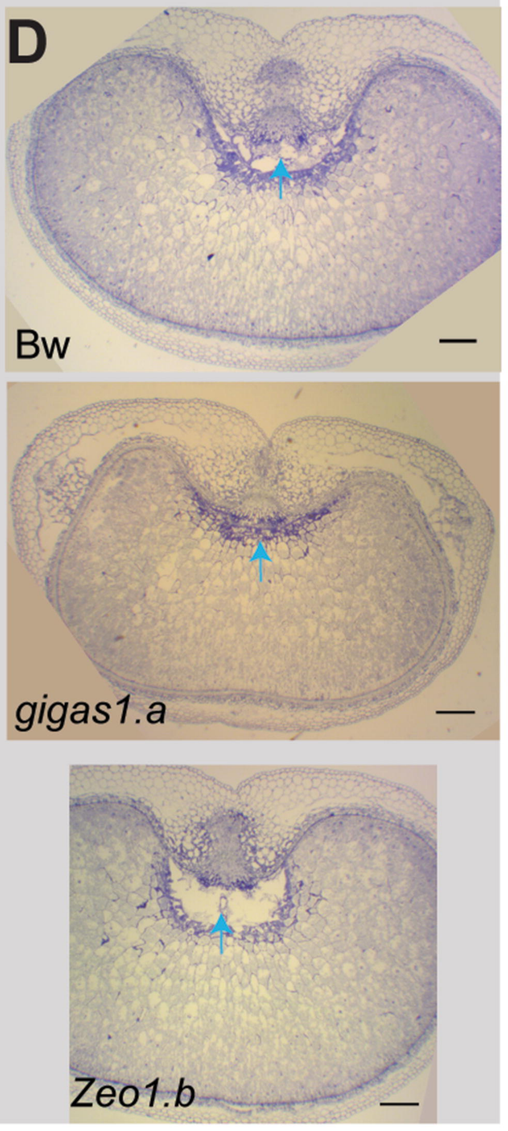

E

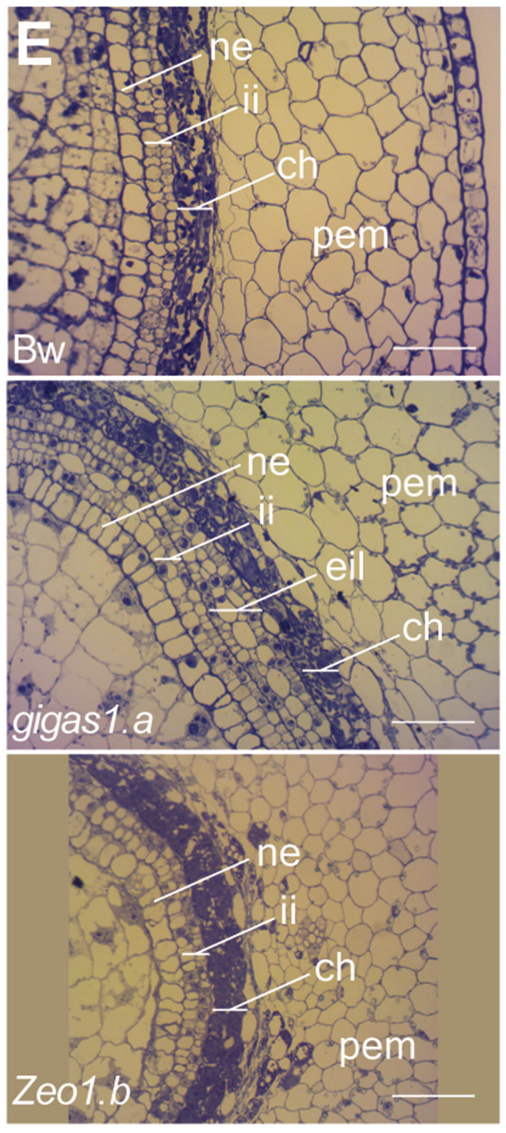

F

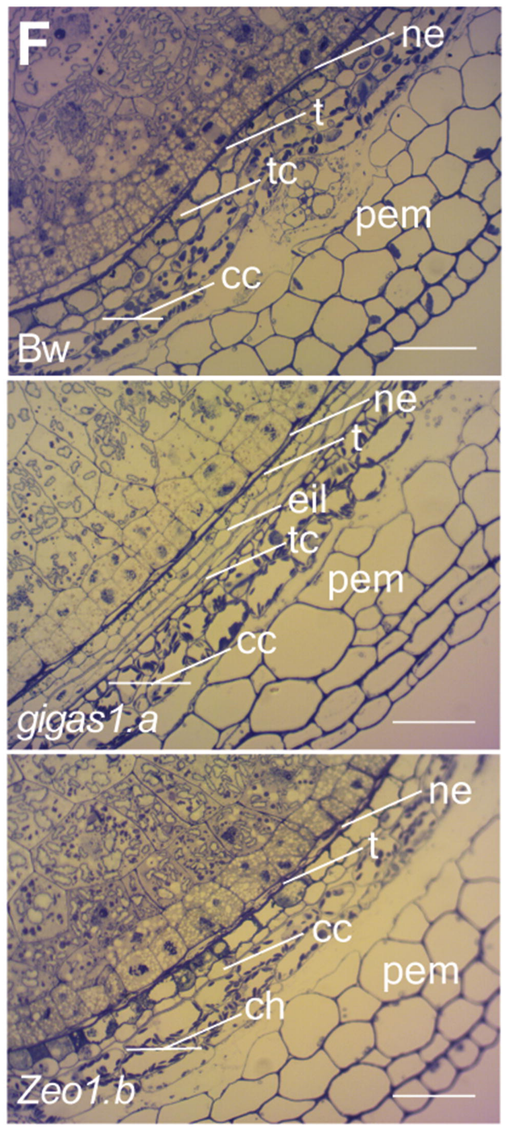

G

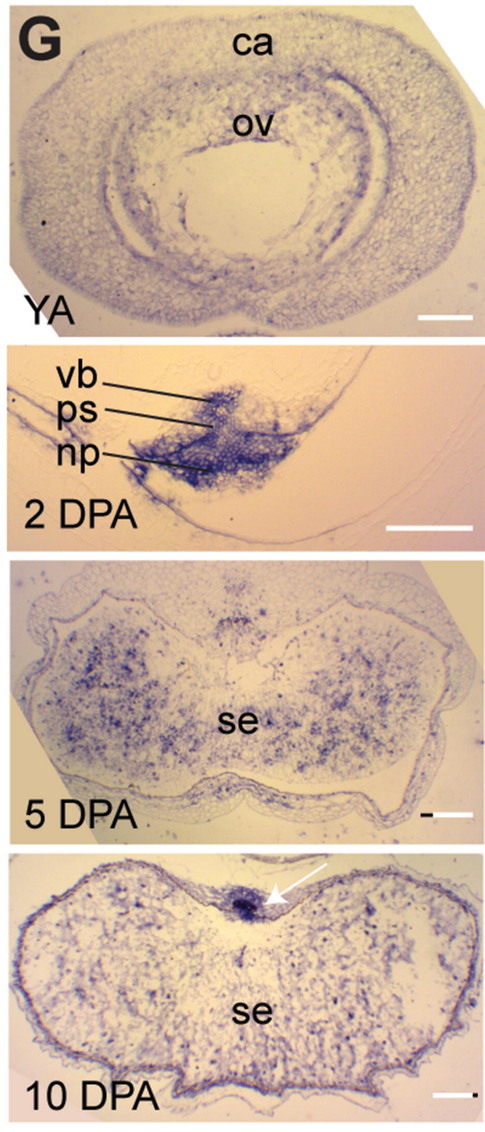

H

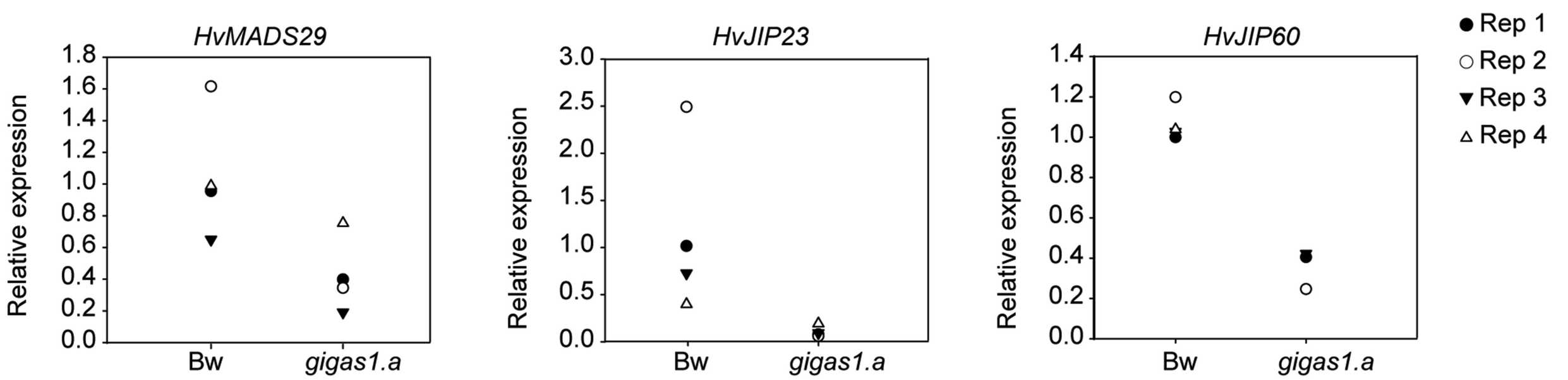

Figure 4

A

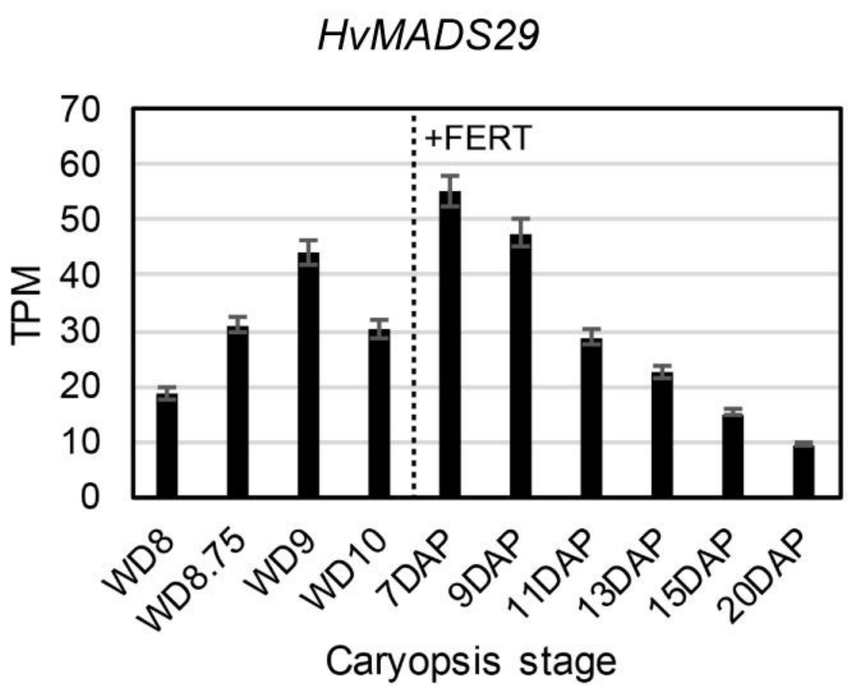
HvMADS29
TPM
70
60
50
40
30
20
10
0
+FERT
WD8
WD8.75
WD9
WD10
7DAP
9DAP
11DAP
13DAP
15DAP
20DAP
Caryopsis stage

B

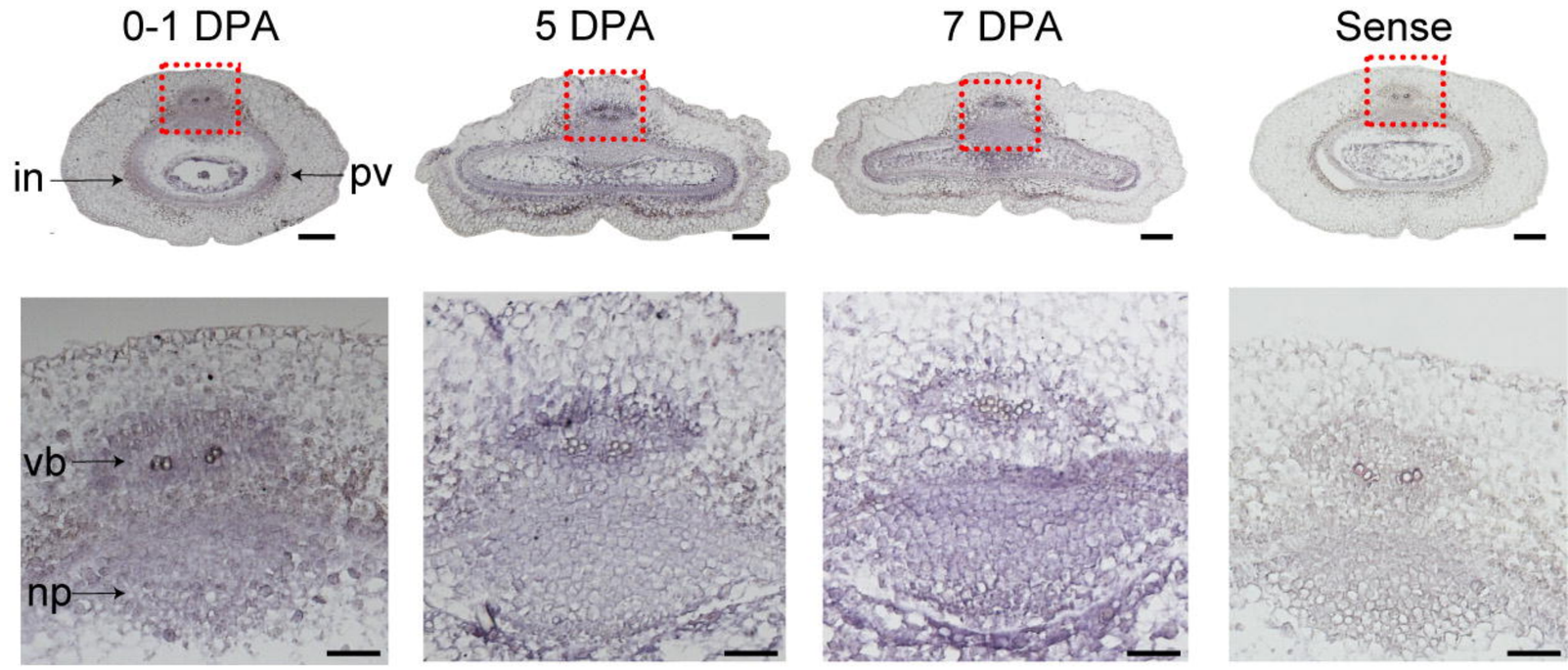
0-1 DPA
5 DPA
7 DPA
Sense
in
pv
vb
np

C

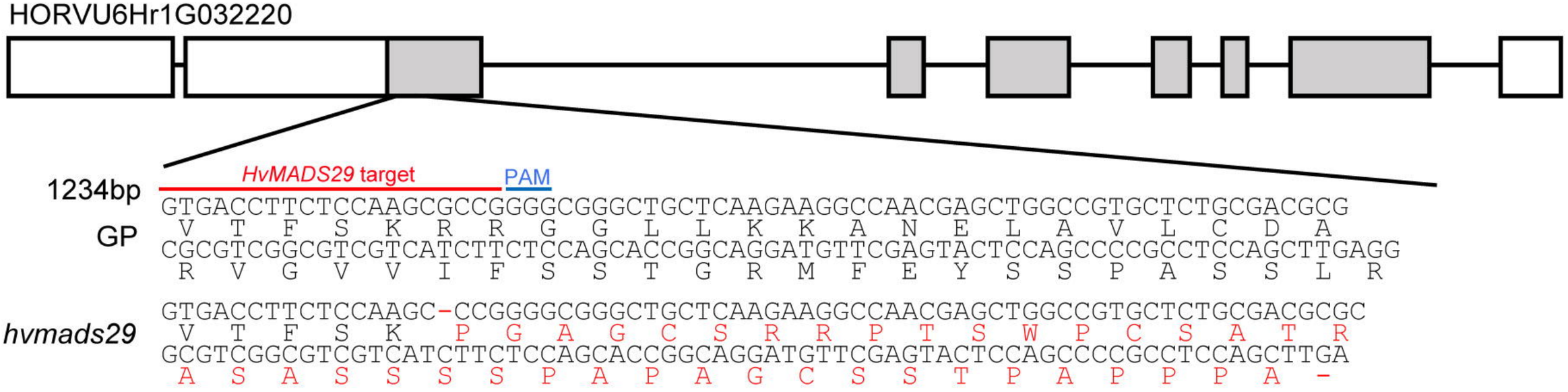
HORVU6Hr1G032220
1234bp
HvMADS29 target
PAM
GP
GTGACCTTCTCCAAGCGCCGGGGCGGGCTGCTCAAGAAGGCCAACGAGCTGGCCGTGCTCTGCGACGCG
V T F S K R R G G L L K K A N E L A V L C D A
CGCGTCGGCGTCGTCATCTTCTCCAGCACCGGCAGGATGTTCGAGTACTCCAGCCCCGCCTCCAGCTTGAGG
R V G V V I F S S T G R M F E Y S S P A S S L R
hvmads29
GTGACCTTCTCCAAGC-CCGGGGCGGGCTGCTCAAGAAGGCCAACGAGCTGGCCGTGCTCTGCGACGCGC
V T F S K P G A G C S R R P T S W P C S A T R
GCGTCGGCGTCGTCATCTTCTCCAGCACCGGCAGGATGTTCGAGTACTCCAGCCCCGCCTCCAGCTTGA
A S A S S S S S P A P A G C S S T P A P P P A -

D

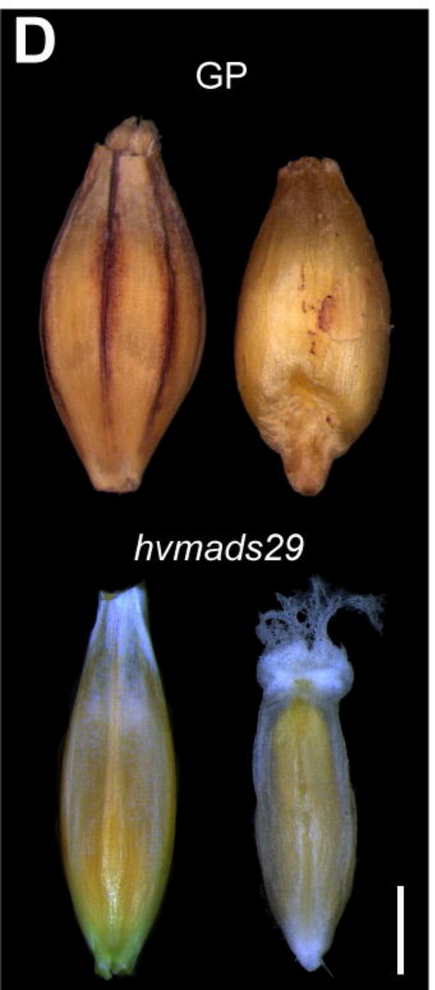
GP
hvmads29

E


GP
hvmads29
0 DPA
5 DPA
10 DPA

F

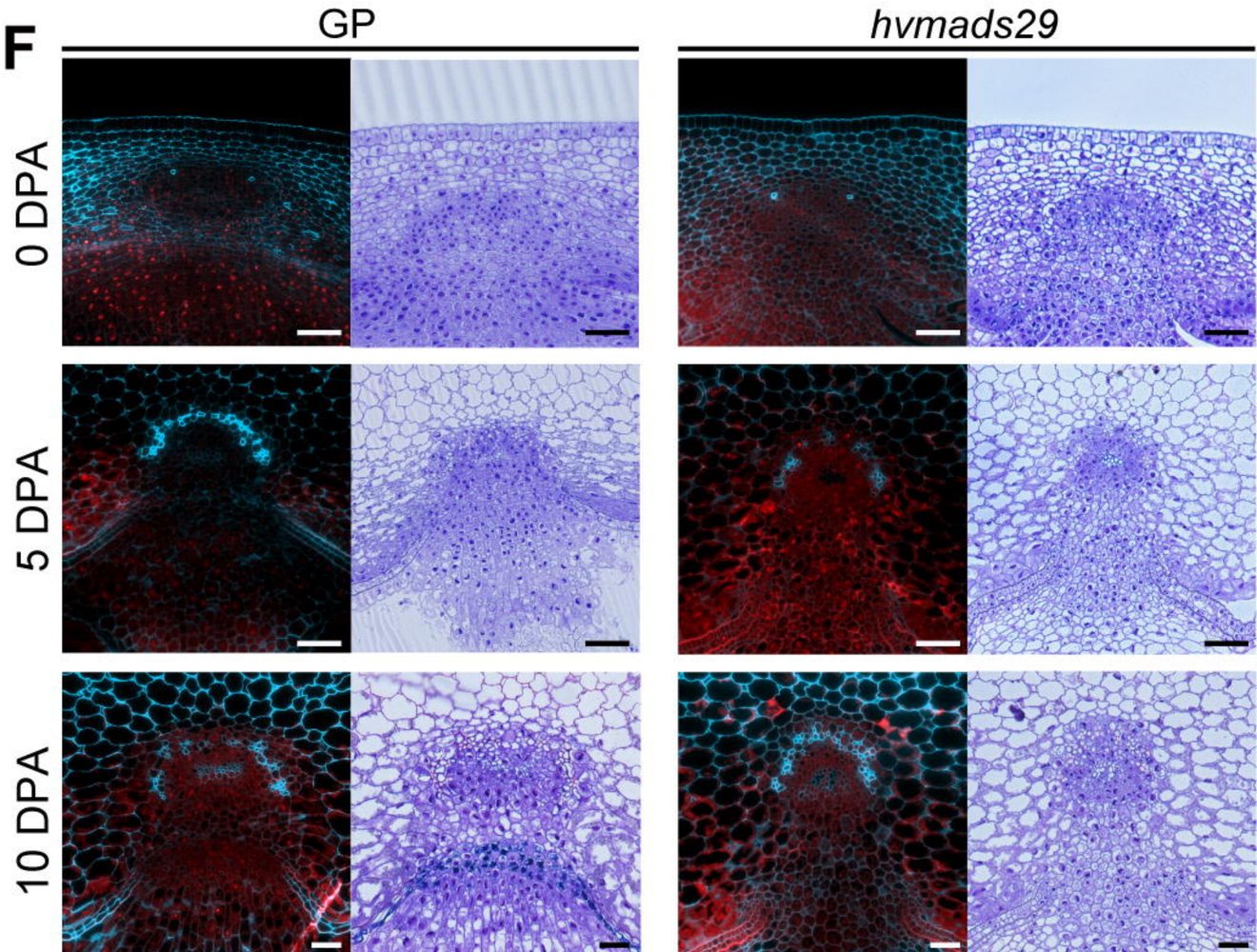
GP
hvmads29
0 DPA
5 DPA
10 DPA

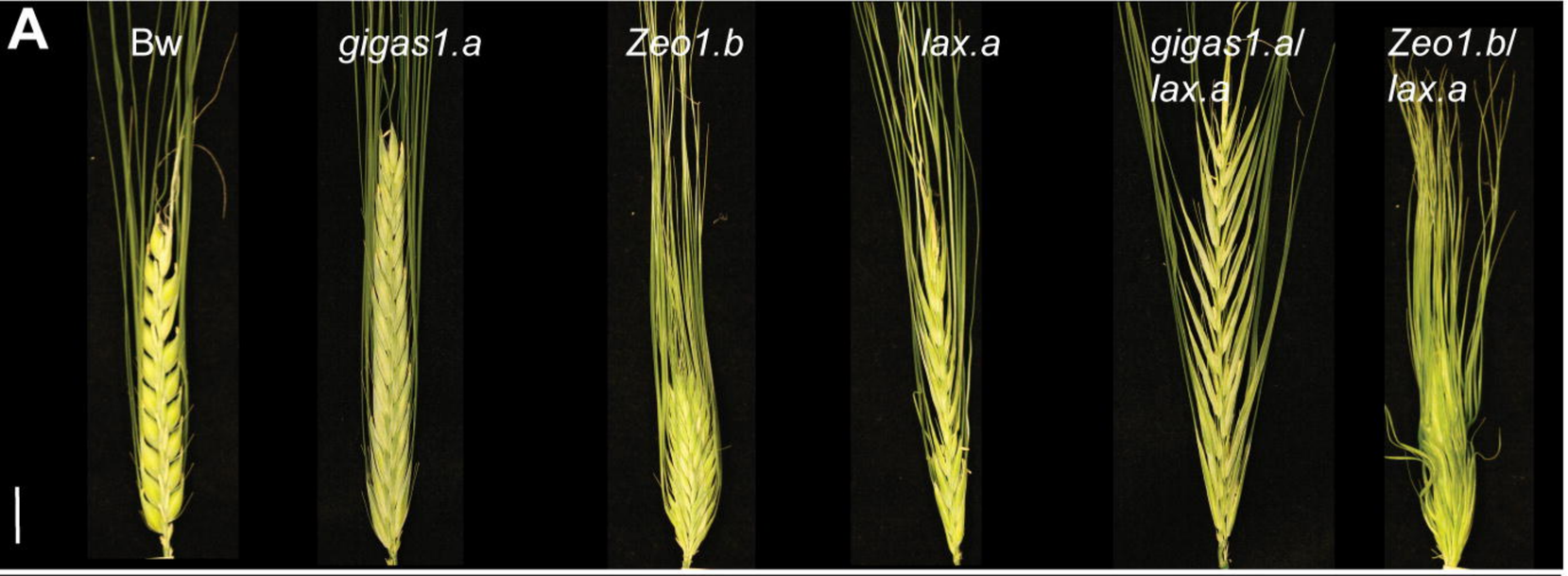

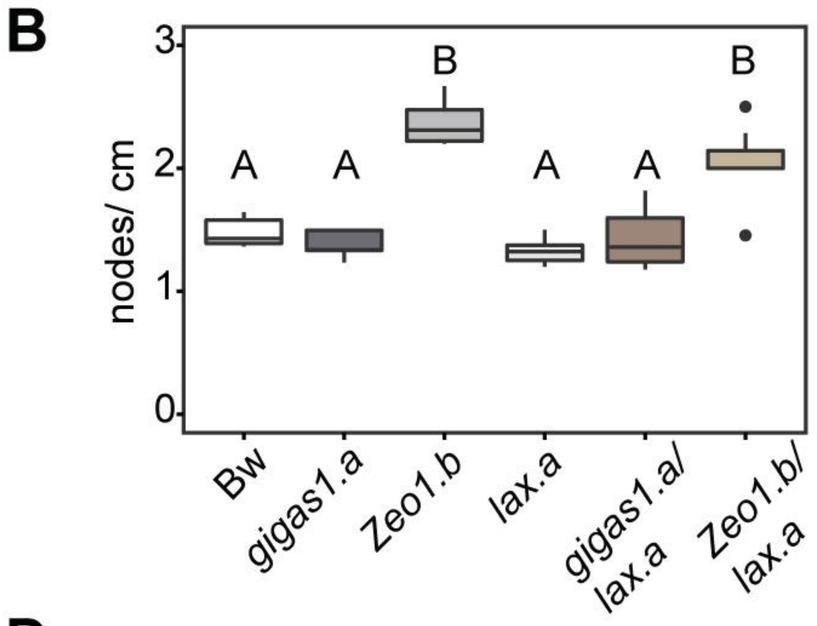

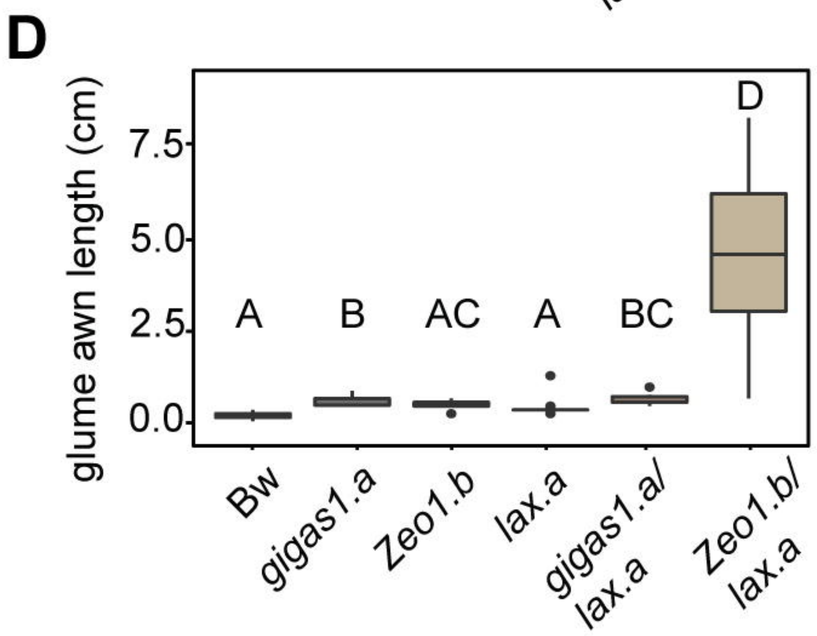

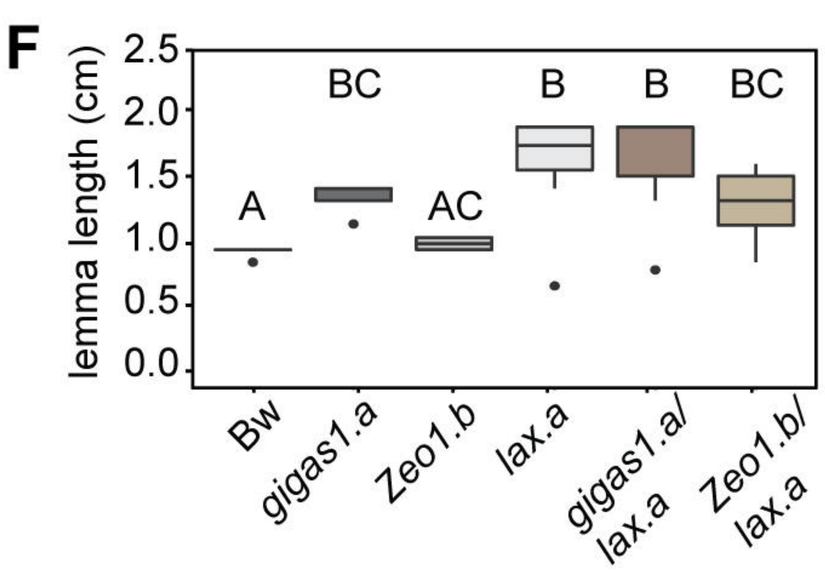

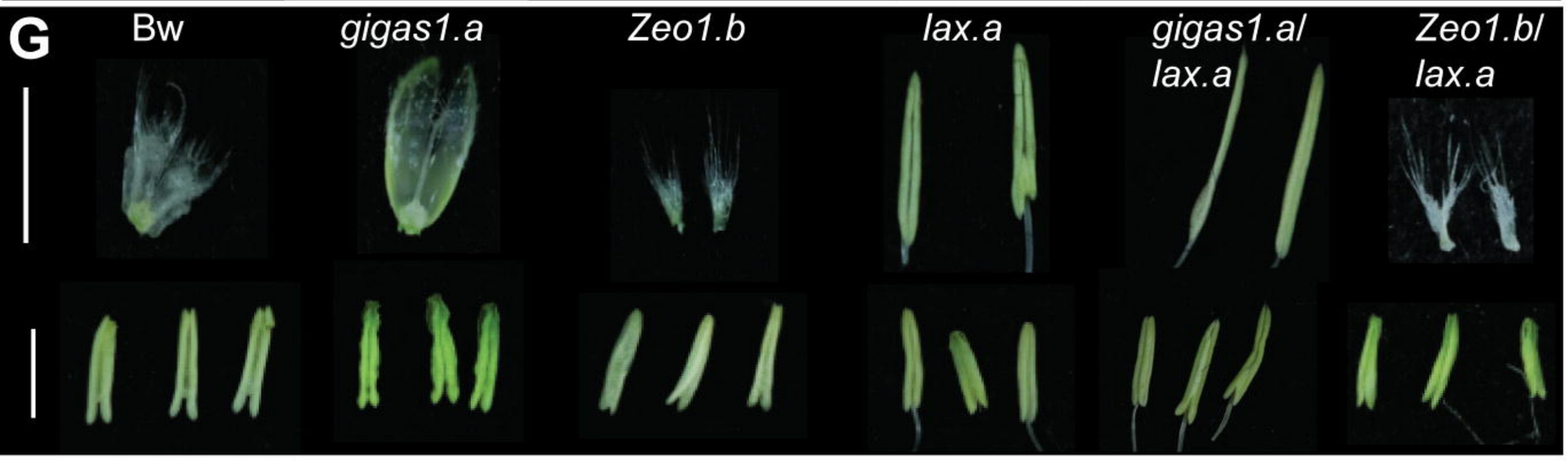

H

	lodicule #	stamen #
Bw	2 ± 0	3 ± 0
gigas1.a	2 ± 0	3 ± 0
Zeo1.b	2 ± 0	3 ± 0
lax.a	0 ± 0	5 ± 0
gigas1.a lax.a	0 ± 0	5 ± 0
Zeo1.b lax.a	2 ± 0	3 ± 0

J

	grain length (mm)
Bw	7.0 ± 0.0^{AC}
gigas1.a	9.9 ± 0.2^{B}
Zeo1.b	6.7 ± 0.0^{AC}
lax.a	7.2 ± 0.1^{A}
gigas1.a lax.a	9.2 ± 0.0^{B}
Zeo1.b lax.a	6.4 ± 0.1^{C}

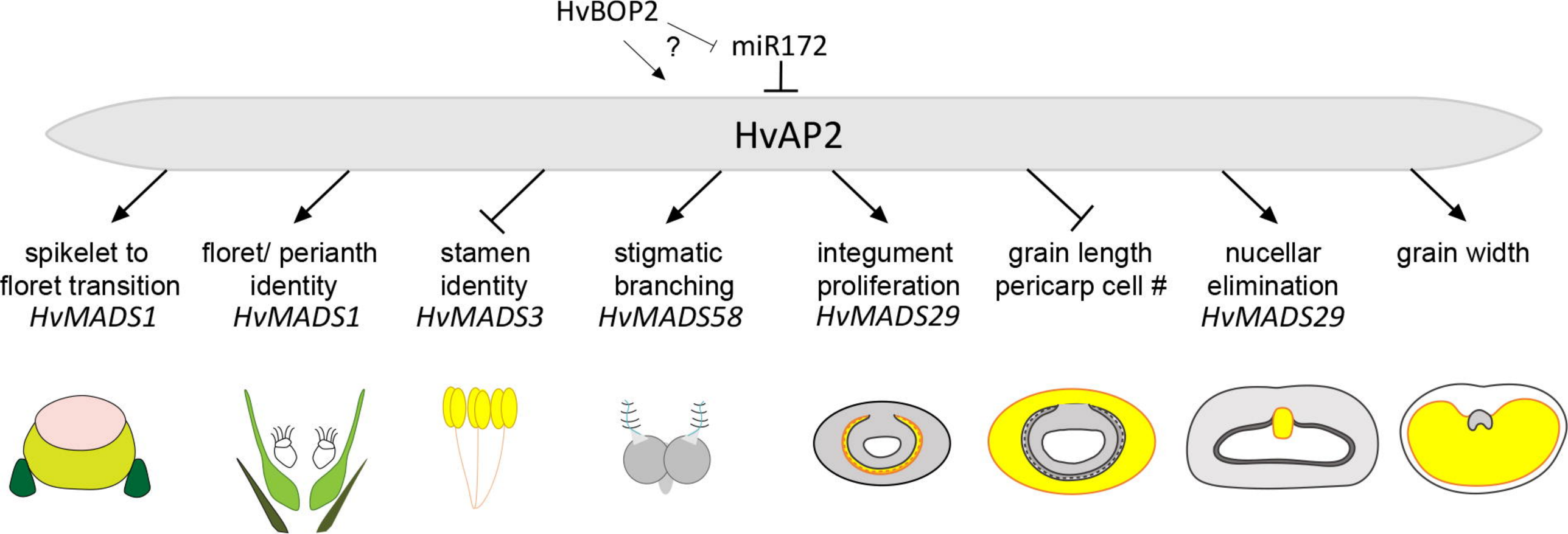
HvBOP2
?
miR172
HvAP2
spikelet to floret transition
HvMADS1
floret/ perianth identity
HvMADS1
stamen identity
HvMADS3
stigmatic branching
HvMADS58
integument proliferation
HvMADS29
grain length pericarp cell #
nucellar elimination
HvMADS29
grain width